PROCESSING AND MECHANICAL TESTING OF Ti6Al4V FOAMS FOR HARD TISSUE IMPLANT APPLICATIONS

A Thesis Submitted to the
Graduate School of Engineering and Sciences of İzmir Institute of
Technology in Partial Fulfillment of the
Requirements for the Degree of

MASTER OF SCIENCE

in Mechanical Engineering

by
Egemen AKAR

August, 2005
İZMİR

We approve the thesis of **Egemen AKAR**

Date of Signature

………………………………….   **12 August 2005**
Assoc. Prof. Dr. Mustafa GUDEN
Supervisor
Department of Mechanical Engineering
İzmir Institute of Technology

………………………………….   **12 August 2005**
Prof. Dr. Muhsin ÇİFTÇİOĞLU
Department of Mechanical Engineering
İzmir Institute of Technology

………………………………….   **12 August 2005**
Assoc. Prof. Dr. Metin TANOĞLU
Department of Mechanical Engineering
İzmir Institute of Technology

………………………………….   **12 August 2005**
Assoc. Prof. Dr. Barış ÖZERDEM
Department of Mechanical Engineering
İzmir Institute of Technology

…………………………………
Assoc. Prof. Dr. Semahat ÖZDEMİR
Head of Graduate School

ACKNOWLEDGEMENTS

ABSTRACT

Sintered Ti6Al4V alloy powder foams were prepared using atomized spherical powders in the porosity range of 52-72 %. For increasing porosity range, space holder was used. Spherical powder foams were cold compacted at (200, 300, 400, 500 MPa) compaction pressures and then sintered at 1200 °C for 2 h and 1300 °C for 2-4-6 h. The final porosities and average pore sizes were determined as functions of the applied compaction pressure and sintered time.

The mean pore size of the foams varied between 94 and 148 μm depending on the particle size range of the powders used and the compaction pressure applied. Microscopic studies of sintered powder foams showed that sintering at high temperature (1200°C and 1300°C) and subsequent relatively slow-rate cooling in the furnace transformed the microstructure of spherical powder from the acicular alpha (α) to the Widmanstätten ($\alpha+\beta$) microstructure.

In compression testing, at quasi-static, the foams failed primarily by shear band formation along the diagonal axis 45° to the loading direction. Microscopic analyses of deformed but not failed and failed spherical powder foam samples further showed that fracture occurred in a ductile (dimpled) mode consisting of void initiation and growth in α phase and/or at the α/β interface and macrocraking by void coalescence in the interparticle bond region.

The strength of the sintered foams was further shown to satisfy the strength requirements for cancellous bone replacement. The strength of the compacts having porosity level of 40% and/or lower was comparable with that of human cortical bone. Compared to Ti powder compacts of previous studies, Ti6Al4V powder compacts provided higher strength and increased porosity level of the foams suitable for cortical bone replacement.

ÖZET

Sinterlenmiş Ti6Al4V toz alaşım köpükler, %52-72 gözenek aralığında, küresel tozlar kullanılarak hazırlanmıştır. Gözenek oranını arttırmak için boşluk yapıcı madde kullanılmıştır. Küresel toz köpükler (200, 300, 400, 500 MPa) basınçlarda soğuk preslenmiş ve 1200 °C – 1300 °C de 2-4 ve 6 saat süresince sinterlenmiştir. Sinterlenmiş köpüklerin gözenek miktarları ve ortalama gözenek boyutları uygulanan presleme basıncı ve sinterleme sürelerine göre tespit edilmiştir.

Köpüklerin ortalama gözenek boyutları 94 ve 148 μm aralığında, kullanılan tozun ortalama tane boyutu ve presleme basıncına bağlı olarak değişim göstermiştir. Sinterlenmiş toz köpüklerin üzerinde yapılan mikroskobik çalışmalar göstermiştir ki, yüksek sıcaklıkta (1200 °C ve 1300 °C) yapılan sinterleme ve ardından fırın içinde uygulanan düşük hızlı soğutmanın sonucu, küresel tozun mikroyapısı iğnemsi alfa (α) dan Widmanstätten ($\alpha+\beta$) yapısına dönüşmüştür.

Statik basma testlerinde köpüklerin, yükleme doğrultusuna 45° açıyla, diyagonal olarak ortaya çıkan kayma bantları oluşumuyla kırıldıkları tespit edilmiştir. Kırılmış ve kırılmamış fakat basma testi sonucu deforme olmuş köpükler üzerinde yapılmış mikroskobik analizler, α fazında ve/veya α/β arayüzeyinde oluşan boşluk oluşumu, büyümesi ve taneler arası bağlanma bölgesinde meydana gelen makro çatlak oluşumu aşamalarını içeren sünek kırılmanın varlığını ortaya koymuştur.

Sinterlenmiş köpüklerin mukavemetinin, süngersi kemiğin yerine geçmesi için yeterli olduğunu göstermiştir. Bunun yanında, %40 ve/veya daha düşük gözenek oranına sahip tabletlerin mukavemetlerinin insan kortikal kemiğinin mukavemetiyle kıyaslanabilir olduğu belirlenmiştir. Daha önceki çalışmalarda üretilen Ti tabletlerle karşılaştırıldığında Ti6Al4V toz tabletler daha yüksek mukavemete ve bu nedenle de kortikal kemik değişimi için uygun olan gözenek miktarının artmasına neden olmuştur.

TABLE OF CONTENTS

LIST OF FIGURES

LIST OF TABLES

CHAPTER 1

INTRODUCTION

The field of biomaterials is becoming one of the most exciting research areas of the materials science and engineering as we enter the 21st century. The activity in the field is not new but there are currently new motivations in this field brought by the advances in molecular and cell biology. Early activities in this field dealt with the selection and characterization of the known synthetic materials to fabricate implants for use in medicine and as restorative materials in dentistry. Materials well established in technology and not originally developed as biomaterials were being used for human repair. For example, bone implants used by orthopedic surgeons were being fabricated from low-corrosion resistant steels and other alloys or from ultrahigh-density polyethylene. Methacrylate polymers were being tested and used as bone cements and dental restoratives, and polyethylene terephthalate fibers were being woven into fabrics that could function as artificial blood vessels. During the early period of this field, cellulose-based membranes were being introduced in kidney dialysis machines. Therefore, biomaterials research was mostly centered on in vitro testing of these materials under conditions that simulated the biological environment (e.g., corrosion, fatigue, creep, wear). Extensive histological work ensued following the implantation of these materials into experimental animals in order to understand the biological response brought by materials in various tissues. Lesser research activities were done to explore the use of alternative materials for similar applications. Therefore, the field focused on the application of materials science principles to materials in biomedical use. With only very few exceptions, biomaterials were synthetic and intended to be permanent implants that substituted for structure and/or function in diseased or traumatized tissues. Biomaterials research was mostly in the hands of engineers, physical scientists, pathologists, and clinicians who brought their skills to these new applications of technological materials "(Weiner 1998)". Synthetic implant materials are currently produced from all variety of materials, metals, ceramics, polymers and their composites.

Metals have a particular importance among the biomaterials since they have superior mechanical properties combined with relatively easy production routes and lower

costs. Many metals, including even copper which is known as a toxic material for human body, have been used in biomedical applications since ancient times. Cobalt (Co) based alloys, stainless steels and titanium (Ti) and its alloys are three major metallic materials widely used in biomedical applications. Ti and its alloys have been recently taken more interest despite to their higher cost and complex production processes than other metals. Their major advantage lies in its inherent corrosion resistance, which is attributable to the spontaneous formation of an oxide layer particularly resistant to many acids and saline solutions. Excellent biocompatibility and fatique properties are other advantages of Ti and its alloys. These superior properties have made Ti and its alloys one of the most important class of materials in orthopedic and dental applications.

Unfortunately, most bulk metallic implant materials currently used in orthopedic applications including Ti and its alloys, suffer from problems of interfacial stability with host tissues and biomechanical mismatch of elastic moduli. These problems stem from weak bonding of implant to the adjacent bone and high elastic modulus of bulk metallic implants. Developments in tissue engineering have demonstrated that these problems can be solved using porous implant components based on biocompatible metallic materials by providing better interaction with bone. This is partly due to higher degree of bone growth into porous surfaces and higher degree of body fluid transport through three-dimensional interconnected array of pores "(Piller 1987)", leading to improved implant fixation. Furthermore, relatively low elastic modulus of porous metals as compared with those of bulk metals is expected to reduce the extent of stress shielding, which causes the well-known *implant loosening,* and hence to prolong implant life-time "(Banhart 2001)".

Open cell Ti foams potentially to be used in biomedical applications were previously prepared using a powder metallurgical process, known as space holder method "(Körner and Singer 2002), (Martin et al. 2000)". This method allows a direct near net-shape fabrication of foamed implant components having elastic modulus comparable with that of natural bone and with a relatively homogeneous pore structure and a high level of porosity (60-80%)"(Körner and Singer 2002), (Martin et al. 2000)". By reducing the "elastic-mismatch" as well as "strength-mismatch" between metallic implant and bone, it is expected to have better performance of implant-bone compound which can be called as "iso-elastic multi-material system". For this purpose several innovative investigations have

been undertaken world-wide. Oh and co-workers "(Wen 2000)" reported that the modulus and bending strength of sintered Ti powder compacts were also comparable with those of human bone. It was further shown by the same authors that the porosity level of sintered Ti compacts suitable for the bone replacement was around 30%, which was in accord with the proposed optimal porosity for the ingrowths of new-bone tissues. The compressive yield strength of sintered Ti compacts was however lower than that of the human cortical bone due to the relatively low yield strength of Ti powder "(Wen 2000)". One way of increasing the yield strength of powder compacts is to use biocompatible stronger Ti alloy powders. This experimental study is therefore conducted to produce stronger sintered powder foams that can potentially be used in biomedical applications (load carrying implants) including human cortical bone replacement. In a previous study, we have shown that the compacts made from Ti6Al4V (Ti64) provided higher compression strength as compared with compacts of pure Ti at the similar porosity levels. The ultimate goal of this work was the optimization of the process and properties of the Ti64 foams to satisfy the bio-mechanical design requirements for certain implants to be used as hard tissue replacement applications such as spinal cages.

CHAPTER 2

CELULAR STRUCTURE AND MECHANICAL
PROPERTIES OF
BONE

2.1. Structure of Bone

Bone is classified as either compact (also referred to as cortical) and spongy (also referred to as cancellous or trabecular). Cortical bone represents approximately 4 times the weight of cancellous bone in any long bone. The basic material comprising cancellous and cortical bone appear identical, thus the distinction between the two is the degree of porosity and the organization. The porosity of cortical bone ranges from 5% to 30 % (mostly in the range 5%-10%) while cancellous bone porosity ranges from 30% to 90 % (mostly in the range 75%-95%). Bone porosity is not fixed and can change in response to altered loading, disease, and aging. There are however three types of cells that contribute to bone homeostasis. Osteoblasts are the bone-forming cell, osteoclasts resorb or break down bone, and osteocytes are mature bone cells. Equilibrium between osteoblasts and osteoclasts maintains bone tissue.

2.1.1. Compact Bone

Compact bone consists of closely packed osteons or haversian systems (Figure2.1). The osteon consists of a central canal called the osteonic (haversian) canal, which is surrounded by concentric rings (lamellae) of matrix. Between the rings of matrix, the bone cells (osteocytes) are located in spaces called lacunae. Small channels (canaliculi) radiate from the lacunae to the osteonic (haversian) canal to provide passageways through the hard matrix. In compact bone, the haversian systems are packed tightly together to form what appears to be a solid mass. The osteonic canals contain blood vessels that are parallel to the

long axis of the bone. These blood vessels interconnect, by way of perforating canals, with vessels on the surface of the bone. The osteons are cylindrical at about 200-250 µm in diameter running roughly parallel to the centerline axis of the bone. Cortical bone is semi-brittle; viscoelastic and anisotropic material, and these material properties are influenced by porosity, mineralization level and the organization of the solid matrix.
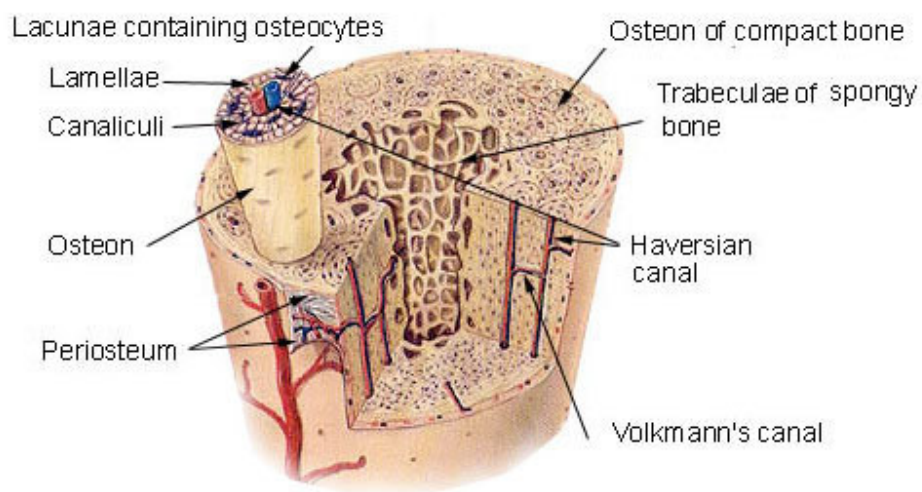
Figure 2.1.   Haversian systems (osteons) in cortical & cancellous bone.

2.1.2. Spongy (Cancellous) Bone

Spongy bone is lighter and less dense than compact bone. Spongy bone consists of plates (trabeculae) and bars of bone adjacent to small, irregular cavities that contain red bone marrow. The canaliculi connect to the adjacent cavities, instead of a central haversian canal, to receive their blood supply. It may appear that the trabeculae are arranged in a haphazard manner, but they are organized to provide maximum strength similar to braces that are used to support a building. The trabeculae of spongy bone follow the lines of stress and can realign if the direction of stress changes. The porous structure of cancellous bone consists of network of marrow filled voids surrounding the trabeculae.

Cancellous bone is active metabolically and is remodeled more often than cortical bone, therefore the mechanical properties of the bone change with age.

2.2. Characterization of Bone

The properties of bone can change significantly if allowed to dry out. Thus, it is very important to keep bone specimens wet during testing. The material properties of bone are generally determined using destructive testing. However ultrasonic techniques have also been employed. Mechanical testing consists of applying tensile, compressive, torsional, or shear loads to bone specimens and recording the deformation of the material. Application of different load types is important since bones undergo different types of loading in vivo. Mechanical testing of bone is really complicated because of the anisotropy (requires multiple samples for testing) and the small sample sizes that are obtainable. For these reasons efforts have been made to use ultrasonic techniques. These techniques make use of the relations between the speed of sound and the elastic properties of the material. Ultrasound requires fewer and smaller specimens to characterize the material properties of bone. The disadvantage is that the relationship between the speed of sound and the tissue's elastic properties must be known.

From the mechanical point of view, cortical bone can be understood as a composite material consisting of at least three phases: the mineralized matrix, the collagen fiber network, and the fluid-filled pore phase.

2.3. Mechanical Properties of Bone

Cortical and cancellous bone mechanical properties are different from each other. Cortical bone is stiffer than cancellous bone and can sustain greater stress but less strain before failure. Cancellous bone can sustain strains of 75 % before failing in-vivo, but cortical bone will fracture if the strain exceeds 2%. Cancellous bone has a greater capacity to store energy compared to cortical bone. It should be stated that the volume fraction of calcium is the dominant factor in determining the mechanical properties; the higher the

volume fraction of calcium the higher the stiffness and strength and the lower the toughness "(Wen 2001)".

The strength and fracture toughness of bone are also time dependent and biological aging and strain rate effect are two major mechanisms in this concern "(WEB_1 2002)".

(i) *Biological aging*. The strength and the modulus of elasticity of bone are affected by aging and decrease after maturation. Moreover, children's bones tend to absorb more energy before failure as compared to adults. Children's bones are weaker, but more compliant.

(ii) Strain rate effect. Ultimate strength and the modulus of elasticity of cortical bone increase with increasing loading or strain rate whereas the ultimate strain decreases. Bone is strain rate sensitive material and tends to be more strain rate sensitive than other biological tissues. At low strain rate, bone behaves like a viscous material. Also, the fracture toughness shows strong strain rate dependence.

Biological materials differ in one respect from other structural materials under repeated loading and unloading. They possess repair mechanisms. Under normal conditions cycling loading of a biomaterial will cause micro-damage. However, damage accumulation will not occur in the case when the repair mechanism is active in a timely fashion. The repair activity can be slowed down for various reasons. Naturally there are age-related changes manifesting as a decrease of bone mineral density. Normal repair can also be impaired by metabolic diseases (e.g., osteoporosis) or by certain drugs. Furthermore, repeated loading without sufficient time for repair activity causes fatigue failure.

Three important parameters that characterize some of the mechanical properties of bone are ultimate force, maximum deformation to failure, and energy that it can store before failure. These properties can be obtained from a force-deformation curve. The ultimate force represents the maximum load that the bone can sustain before it breaks. The ultimate force varies depending on the type of load applied (e.g. tensile, compressive, shear) and the loading rate. The energy absorbed before failure can be calculated from the area under the force-deformation curve and therefore depends on both the ultimate force and the ultimate strain.

2.4. Replacement of Bone

Synthetic or natural materials for the replacement of bones or bone tissue are an essential phenomenon for biomedical application field. Replacing or augmenting bone with an implant can relieve the pain caused by trauma or disease. Replacement of bone occurs in joint arthroplasty or in bone grafting. Augmentation of bone with fixation devices is required for fracture healing, or for stabilization and fusion of joints, or for alignment/distraction of bones. Bone prostheses must address several design requirements "(Clemow et al.1981)".

Among these are:

(i) fit a wide anatomic range of patients,
(ii) maintain mechanical fixation under cyclic loading,
(iii) offer a functional range of motion,
(iv) provide the required kinematic stability.

The relative importance of the design requirements depends on the function of the implant. Design of surgical procedures and associated instrumentation is also an essential aspect to the development of bone prosthesis systems. The design requirements for bone prostheses are met firstly by the selection of suitable biomaterials. These must have the required biocompatibility, i.e., perform with an appropriate host response in a specific situation. Sometimes the implant must remain strictly inert to facilitate removal from the body, e.g., a fixation plate. Other implants must resorb over time, and others are designed to 'osseointegrate' with the host bone - osseointegration being a process of bone ingrowth at the implant surface to create a secure bond with the bone. Secondly, the geometry of the implant is a critical factor because it determines the stress distribution at the bone/implant interface and within the surrounding bone. In the case of joint replacement prostheses, the geometry of the articulating surfaces determines the range of motion of the prosthetic joint, and the kinematic stability of the articulation. The regulatory environment for new implants plays a critical role in determining the evolution of new designs.

Artificial scaffolds are examples of this new trend implants and directly affect the formation of bone tissue. Hence, this scaffold should meet some requirements for the regeneration of bones. The major chemical requirement for the scaffold is its biocompatibility, the absence of any inflammatory response or toxicity upon implantation of scaffold. In addition to biocompatibility, the scaffold should support growth of bone cells into a three dimensional structure to form bone. Surface energy may play a role in interaction of proteins with the surface of the material thus affecting the affinity of the cells to the material. Particle size, shape and surface roughness also influence cellular adhesion and proliferation. The macrostructure of the scaffold should mimic the physiological functions of the native extra cellular matrix for cells so that they differentiate and proliferate properly. Interconnected porous structure is required to provide necessary space for cell ingrowth and vascularization. The optimum pore size varies from 200 to 500 µm depending on the tissue to be replaced "(Chang et al. 1996)". The interconnective structure should allow uniform cell distribution, cell survival proliferation and migration. In particular it should allow free passage of body fluids, nutrients and gases to the cells and removal of metabolic waste and by products from cells. High internal surface area to volume ratio is essential to accommodate a large number of cells.

Scaffolds should possess a high mechanical strength until the new tissue is formed completely in addition to its macrostructure and biocompatibility properties. They should be strong enough to tolerate any in vivo stresses and physiological loadings that are imposed on them. The implants should also be supplied at any time and in any quantity. It is difficult to define standards for tissue engineering scaffolds due to the diverse characteristics such as pore size, total porosity, pore shape, pore interconnectivity, material surface chemistry, effective scaffold permeability and scaffold's stiffness that can affect bone regeneration.

CHAPTER 3

THE PROCESSING METHODS OF POROUS METALS FOR BIOMEDICAL APLICATIONS

3.1. Productions Methods of Cellular Metallic Materials

Foams and other highly porous materials with a cellular structure are known to have many interesting combinations of physical and mechanical properties, such as high stiffness in conjunction with very low specific weight or high gas permeability combined with high thermal conductivity. For this reason, nature frequently uses cellular materials for constructional or functional purposes (e.g. wood or bones). Among man-made cellular materials, polymeric foams are currently the most important ones with widespread applications in nearly every sector of technology. Less known is that even metals and alloys can be produced as cellular materials or foams and that these materials have such interesting properties that exciting new applications are expected in the near future. Cellular solids and their properties have been described in much detail by Gibson and Ashby "(Gibson and Ashby 1997)". A frequently cited review of cellular metallic materials was published in 1983 "(Elbir et al. 2003)". Since then, many new developments concerning the production, characterization and application of metal foams have occurred.

According to Figure3.1 which lists the designations for all possible dispersions of one phase in a second one (where each phase can be in one of the three states of matter), foams are uniform dispersions of a gaseous phase in either a liquid or a solid "(Weiner 1998)". The single gas inclusions are separated from each other by portions of the liquid or solid, respectively. Thus the cells are entirely enclosed by the liquid or solid and are not interconnected. The term foam in its original sense is reserved for a dispersion of gas bubbles in a liquid. The morphology of such foams, however, can be preserved by letting the liquid solidify, thus obtaining what is called a solid foam.

Figure 3.1   Dispersions of one phase into a second one. Each phase can be in one of the three states of matter (Source: Weiner 1998)".

Metallic foams mean solid foam. The liquid metallic foam is merely a stage that occurs during the fabrication of the material. Solid foams are a special case of what is more commonly called a cellular solid. As in a liquid the minimization of surface energy only allows for certain foam morphologies, the solid foam, which is just an image of its liquid counterpart, is restricted in the same way. In contrast, cellular solids are not necessarily made from the liquid state and can therefore have nearly any morphology, e.g. the typical open structure of sintered powders. Often such porous structures are also named foams.

There are many ways to manufacture cellular metallic materials. Some methods are similar to techniques used for foaming aqueous or polymer liquids, whereas others are specially designed by taking advantage of characteristic properties of metals such as their sintering activity or the fact that they can be electrically deposited. The various methods can be classified according to the state the metal is processed in. The processes are summarized in Figure 3.2 each one corresponding to one of the states of matter: one can start

(i) from solid metal in powdered form,

(ii) from liquid metal,

(iii) from metal vapor or gaseous metallic compounds,
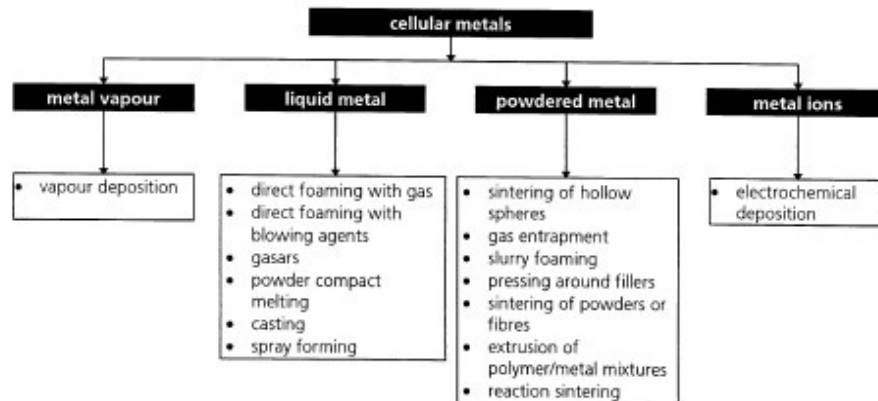
11

(iv) from a metal ion solution.

Figure 3.2.   Overview of the various ''families'' of production methods for cellular metallic materials.

3.1.1. Solid State Processing of Cellular Ti for Biomedical applications

Although, melting methods have been successfully applied to the manufacture of Al, Zn and Mg foams, they are not suitable for the manufacture of Ti foams due to the high melting temperature and reactivity of Ti. In the PM approach, designed structures are manufactured either by sintering of hollow spheres or by melting or partial melting of powder compacts that contain a gas evolving element (e.g.TiH_2) "(Banhart 2001)". Since these methods unavoidably result in enclosed pores (closed cell foam), they are also not suitable for the manufacture of foamed metal implants because of the requirement of body fluid transport. Open cell implant foam metals can be however successfully manufactured by a versatile PM based process known as space holder method "(Martin et al. 2000), (Wen 2001)". The method can be used to manufacture fully and/or partially (as coatings on solid implants for bone fixation) foamed biomedical metals. The size, level and geometry of pores can be easily altered by varying the size, amount and shape of space holder. Therefore, it is one of the appropriate methods for manufacturing designed foam metal implants.

The processing steps of space holder method are schematically presented in Figure3.3. The process starts with mixing of metal powders with a suitable space holder material, followed by a compaction step (e.g. uniaxial and isostatic pressing) that produces metal powder-space holder mixture compact. The green compact is then heat treated at a relatively low temperature to release the space holder, resulting in an unfired open cell foam metal structure. Finally, the compact is sintered at relatively high temperatures to provide structural integrity. This method allows a direct near net-shape fabrication of foamed implant components with a relatively homogeneous pore structure and a high level of porosity (60-80%).

Ti or Ti-6Al-4V powder   Space holder

Mixing with solvent

Compaction

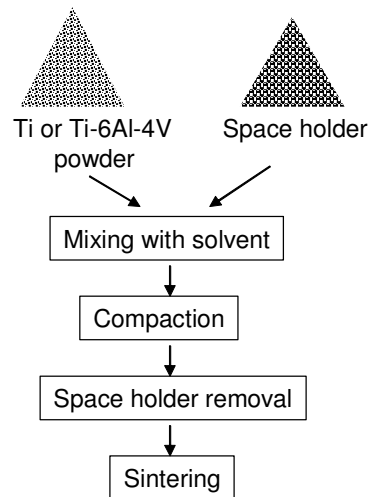Space holder removal

Sintering

Figure 3.3.   Processing steps of space holder method.

Ti and its alloys are known to be very reactive and can easily form interstitial solid solutions with other elements including carbon, oxygen and nitrogen. Since the presence of these elements is detrimental for the ductility, the reaction between Ti powder and the cracking products of the space holder in a temperature range of 300-600 $^{\circ}$C must be avoided "(Martin et al. 2000), (WEB_1 2002)". It is therefore proposed that space holder should be removed at temperatures below about 200 $^{\circ}$C "(Martin et al. 2000)". Ammonium hydrogen carbonate and carbamide (urea) are the materials identified to satisfy this criterion

13

and currently used for the processing of Ti foams "(Wen 2001)". The optimum pore size range required for the attachment and proliferation of new bone tissue and the transport of body fluids is given to be between 200 and 500 μm "(Clemow et al.1981)"; therefore, the particle size range of space holder must be selected and/or tailored according to the critical pore size range. In the design of foam metal final pore size range, however, pore shrinkage occurring during sintering should also be taken into consideration. For the preparation of highly porous foam parts, the particle size distribution of metal powder should be lower than the average particle size of space holder "(Martin et al. 2000)". A particle size lower than 150 μm is normally sufficient for the homogeneous coating of 200-500 μm size space holder particles with Ti powder. Furthermore, the consolidation pressure of metal powder-space holder mixture must be high enough for the preparation of mechanically strong compacts that would retain their geometry throughout the foaming process. The compaction of Ti powder is usually conducted under a uniaxial pressure ranging between 100 and 200 MPa, while higher pressures, or a binder material, may be required for the compaction of the harder Ti-6Al-4V powder.

3.1.2. Characterization

Cellular metals and alloys can be characterized in many ways. The objective is either to obtain mechanical or physical data characteristic of the cellular material investigated or to carry out a technological characterization of a component containing cellular metal. Cellular material is a construction consisting of a multitude of struts, membranes or other elements which themselves have the mechanical properties of some bulk metal. Testing a cellular material is therefore equivalent to testing any engineering component. Hence, a cellular structure can be considered as a homogeneous medium which is represented by averaged material parameters.

The overall density of a porous material can be determined by weighing it and by measuring its volume using Archimedes' principle. According to this principle liquid should not be penetrated into pores of metal. If the sample to be characterized does not have a closed outer skin, penetration of liquid into the pores has to be prevented by coating its surface with a polymer or paraffin film.

The liquid processing methods yield cellular materials with closed cells or even a closed outer skin. However, in practice imperfections occur while making the foams such as in the cooling stage after processing. Such imperfections can include little holes or cracks in the cell walls or in their outer skin. Penetration techniques are ideal for detecting such surface defects. In this technique, a liquid chemical is firstly applied to the cellular metal to be investigated. The chemical is eventually absorbed by the holes and cracks. After drying the surface, a coloring developer is applied which creates color where the penetrant chemical has been retained. In this way, maps of the imperfections can be obtained in a simple visual manner.

3.1.3. Optical Image Analysis

The cell morphology and microstructure of cellular metals can be analyzed by microscopy observations at various magnifications. Although the actual analysis is nondestructive, sample preparation usually requires cutting, embedding or polishing of the materials and is therefore effectively a destructive technique. Optical image analysis programs help to investigate structure photographs of cellular materials taken by optic or electron microscopes.

Cell or pore size distributions can be determined or a shape analysis of the cells can be performed by using commercial image analysis programs. A very careful preparation of the materials is required to obtain reasonable analysis results. In optical image analysis, cell membranes and the interior of the cells must appear in different brightness. One way is to embed the cellular material in a black resin and to polish the preparation plane. This process which is treated to obtain more contrast between pores and cell walls is given in Figure 3.4.
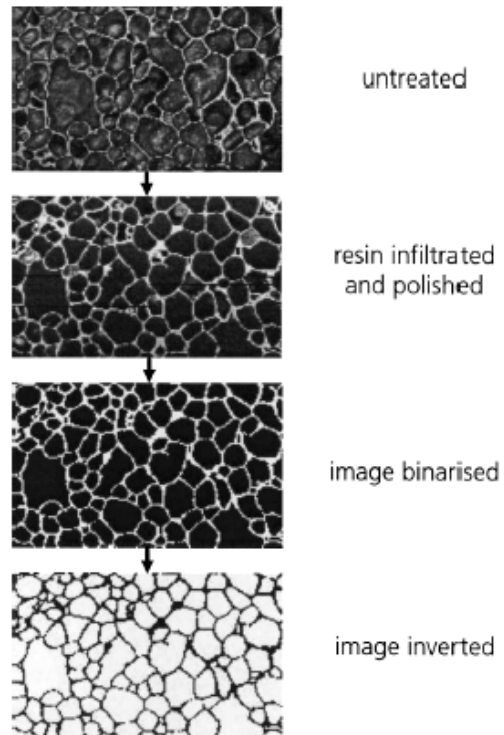
untreated

resin infiltrated
and polished

image binarised

image inverted

Figure 3.4.   Sample preparation in image analysis.

CHAPTER 4

MATERIALS AND TESTING METHODS

4.1. Materials

The sintered powder foams were prepared using Ti6Al4V alloy powders; atomized spherical particles were manufactured by Phelly Materials with atomization process. The chemical composition of Powder complied with ASTM 1580-1 standard "(Kulkarni and Ramakrishnan 1973)" is tabulated in Table 4.1. Moreover, the chemical composition of powder given by producer Company is shown in the same table. The particle size of powder ranged between 23 and 90 μm with a mean particle size of 70.5 μm. The particle sizes of space holder (amonium bi carbonate) ranged between 350 and 500 μm with a mean particle size of 170 μm. The powders and space holders were sieved in the particle size range of <90μm, and 315-500 μm in order to determine the effect of particle size on the porosity attained in the powder foams. Mean powder sizes were microscopically measured as 70 for Ti6Al4V powder and 170 μm for space holder. The SEM images of powders sieved <90μm and 350-500μm are shown sequentially in Figures 4.1 and 4.2 for Ti6Al4V powder and space holder respectively. Ti6Al4V powder particles are spherical and nearly uniform particle size. Space holder particles are almost spherical.

Table 4.1.   ASTM standard for Ti6Al4V powder and chemical composition of the powder.

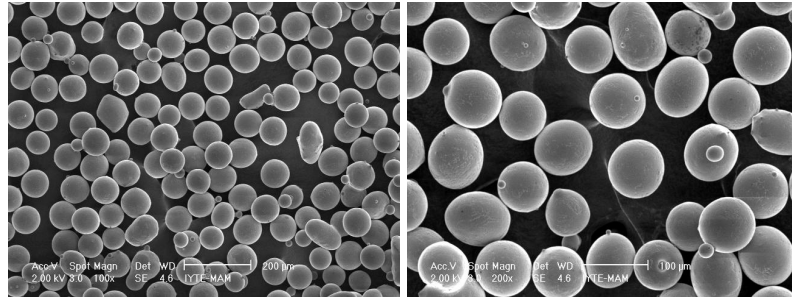| Element	Al	V	O	Fe	C	H	N	Cu	Sn	Ti
ASTM F1580-01	5.5~6.75	3.5~4.5	0.2	0.3	0.08	0.015	0.05	0.1	0.1	Balance
Testing Results	6.13	3.89	0.17	0.11	0.02	0.013	0.024	<0.05	<0.05	Balance

Figure 4.1.   SEM micrographs of Ti6Al4V powder (<90μm)
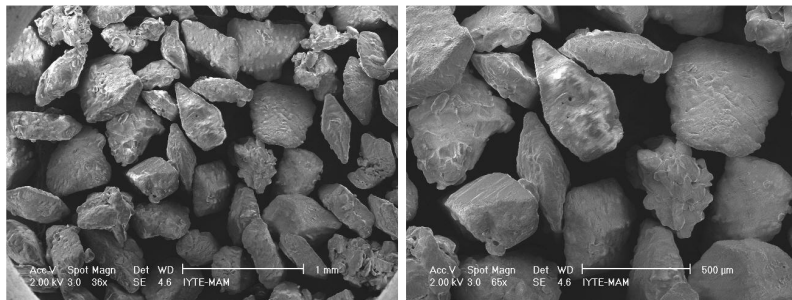

Figure 4.2.   SEM micrographs of space holder, 315-500 μm.

4.2. Foam Compaction

Before compaction powder was mixed with 52-62-72 volume % of amonium bi carbonate and PVA solution 10% by volume was used as the binding material. The mixture was then compacted at room temperature inside a steel die. The green compacts were 10 mm in length and 15 mm in diameter. It was found that without using a binder the powder could not be shaped until about the pressures of 200 MPa; therefore, PVA solution 10% by volume was used as the binding material in an amount of 10% by weight. Compaction pressures chosen for foams were 200, 300, 400 and 500 MPa. Before sintering space holder was removed at 200 ^{o}C for 5 hours. The sintering of compacts was performed in a tightly enclosed horizontal tube furnace under the high purity (99.998%) Ar atmosphere at two different temperatures, 1200 and 1300 ^{o}C, and at different sintering times, 2, 4 and 6 h. The sintering temperature and time were chosen based on the previous sintering studies of Ti foam and powder compacts "(Martin et al. 2000), (Wen 2000)". The compacts were

inserted into the furnace at room temperature inside an enclosed Ti6Al4V box on a graphite plate which prevented the bonding between Ti6Al4V box and foams. The compacts were heated and cooled with a rate of 5 $^{\circ}$C per min. In the heating cycle, the foams were kept at 450 $^{\circ}$C for ½ hour in order to allow the burning of the binder.

4.3. Compression Testing

Quasi-static compression tests were performed on the cylindrical foam samples, 15 mm in diameter and 10 mm in length using a displacement controlled SHIMADZU AG-I universal tension-compression test machine,. Eccentric compression test plate was used in all tests in order to prevent shear forces formed by uneven surfaces of the test specimens (Figure 4.3). Tests were performed at a cross-head speed of 2 mm min^{-1} corresponding to a strain rate of 2×10^{-3} s^{-1}, respectively. During compression test, the test plates and surfaces of the samples were lubricated in order to reduce the friction between sample and the test plates. At least three tests were conducted for each set of powder samples. Elastic modulus, yield stress, ultimate compressive stress and failure strain values were determined from the determined stress-strain curves. The measured strain values were corrected with the compliance of the compression test machine.
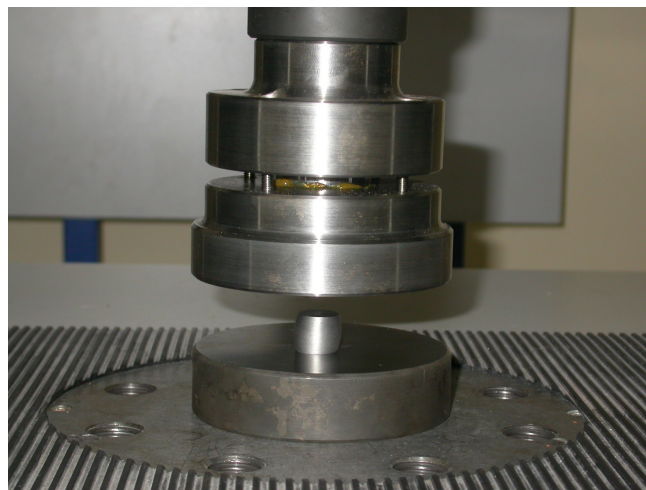

Figure 4.3.   Eccentric compression testing apparatus.

4.4. Microscopic Studies

Compression tested and untested foam samples were investigated under optic microscope and Philips XL30-SFEG scanning electron microscope (SEM) with an Energy Dispersive X-ray (EDX) analyzer, on the vacuum epoxy-mounted. Vacuum mounting was performed using vacuum mounting equipment as shown in Figure 4.5. In the mounting process, 200 ml epoxy was mixed with 1ml initiator and 2 ml accelerator and then poured onto the foams under vacuum atmosphere. The polished cross-sections of samples were etched with Kroll's reagent (3 cm^3 of HF and 6 cm^3 of HNO$_3$ in 100 ml of H$_2$O). The percent porosity of sintered foam was measured by the Archimedes' method. The open and closed porosities of foams were calculated by the differences between dry and wet weights.

Figure 4.4.   Vacuum - mounting equipment.

4.5. Porosity and Pore Size Measurements

Porosity measurements were performed by the Archimedes' method after coating the surface of the compacts with paraffin to prevent penetration of water into the pores. After measuring the density of the compacts, porosities (P) were calculated via density values by using the following equations;

$$P = 1 - \rho_{rel} \quad\quad\quad (4.1)$$

$$\rho_{rel} = \frac{\rho_{foam}}{\rho_{solid}} \quad\quad\quad (4.2)$$

Where, ρ_{rel} is the relative density of the compact, ρ_{com} is the density of compact and ρ_{solid} is the density of Ti6Al4V. To determine the mean pore size of sintered Ti6Al4V, foams were transversely cut and epoxy-mounted. Mean pore sizes of the compacts were calculated applying the linear intercept method on the images of the polished surface of the compacts using a Nikon Eclipse L150 optical microscope. At least 5 random lines were drawn onto the image of the powder compact and then pore sizes intercepting with the random lines were measured.

CHAPTER 5

RESULTS AND DISCUSSIONS

5.1. Microstructure of the as-received Ti6Al4V Powders

The microstructure of as-received powder (Figures 5.1 (a) and (b)) consists of acicular needle-like α which is known as martensitic α. This type of microstructure can form as a result of fast cooling (quenching) after heat treatment above β-transition temperature during atomization process. EDAX analysis has confirmed approximate composition of the alloy as shown in Figure 5.2.

(a)	(b)
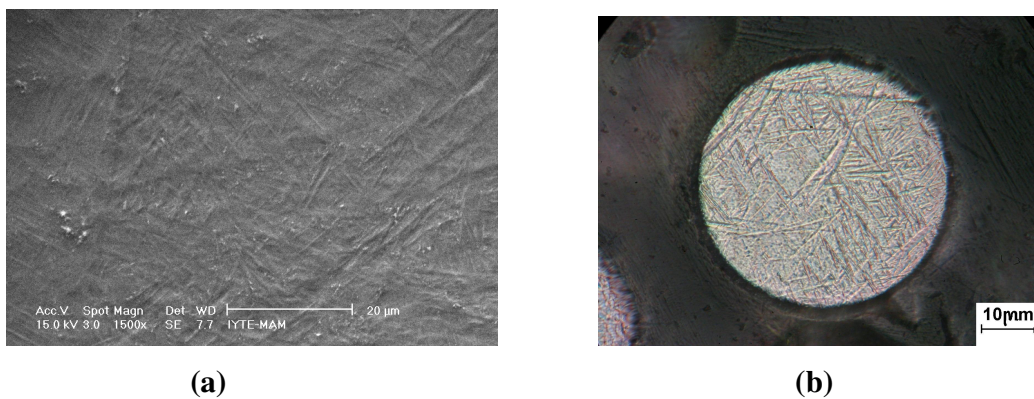
Figure 5.1.   (a) Optical and (b) SEM micrographs of Ti6Al4V powder.

5.2. Thermogravimetry Analysis of Polyvinyl Alcohol (PVA)

Thermogravimetry analysis (TGA) curve of PVA used as binder in the compaction of powders is shown in Figure 5.2. The test was performed at a rate of 5 °C min^{-1}, the same as that of the heating rates of powder compacts. As depicted in Figure 5.2,

the burning of PVA starts at a temperature of nearly 280 °C and continues up to 500 °C. In accord with TGA curve shown in Figure 5.2, the compacts prepared with PVA were kept for ½ hour at 450 °C in order for removal of PVA.
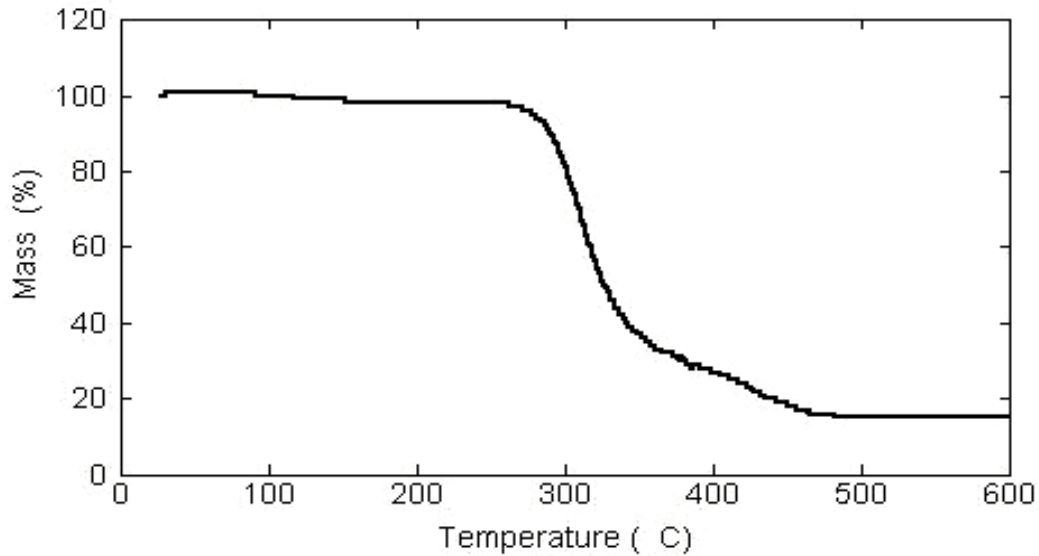
Figure 5.2.   TGA curve of polyvinyl alcohol (PVA).

5.3. Porosity and Pore Size Measurements

The porosity values of the foams prepared are tabulated in Table 5.1 together with applied the compaction pressures, space holder ratio, sintering temperature and sintering time. The cold compaction pressure has a significant effect on the final measured porosity of the foams. Increasing compaction pressure, sintering temperature and sintering time increases the relative density of foams by providing higher contact areas between particles, leading to decrease in final foam porosities. The porosity levels of the foams vary between 49% and 73% (Table 5.1). The mean pore sizes of the foams range between 94 and 148 μm.

Table 5.1.   Compaction pressures, space holder ratio, sintering temperature, sintering time, porosity and mean pore size of the prepared foams.

Compaction Pressure (MPa)	Space Holder Ratio (%)	Sintering Temperature (°C)	Sintering Time (h)	Porosity (%)	Mean Pore Size (µm)
200	62	1200	2	64	148
300	62	1200	2	63	137
400	62	1200	2	63	123
500	62	1200	2	62	113
300	62	1300	2	61	132
500	62	1300	2	60	110
700	62	1300	2	58	98
700	62	1300	4	57	94
500	62	1300	4	61	108
500	62	1300	6	58	99
500	72	1300	6	73	105
500	52	1300	6	49	111

The optical microscope images of the polished surfaces of Ti6Al4V foams at changing cold compaction pressures, sintering temperatures and times are shown in Figure 5.3 to 5.12. It is noted from these micrographs the foam pore size decreases with increasing compaction pressure and sintering times.
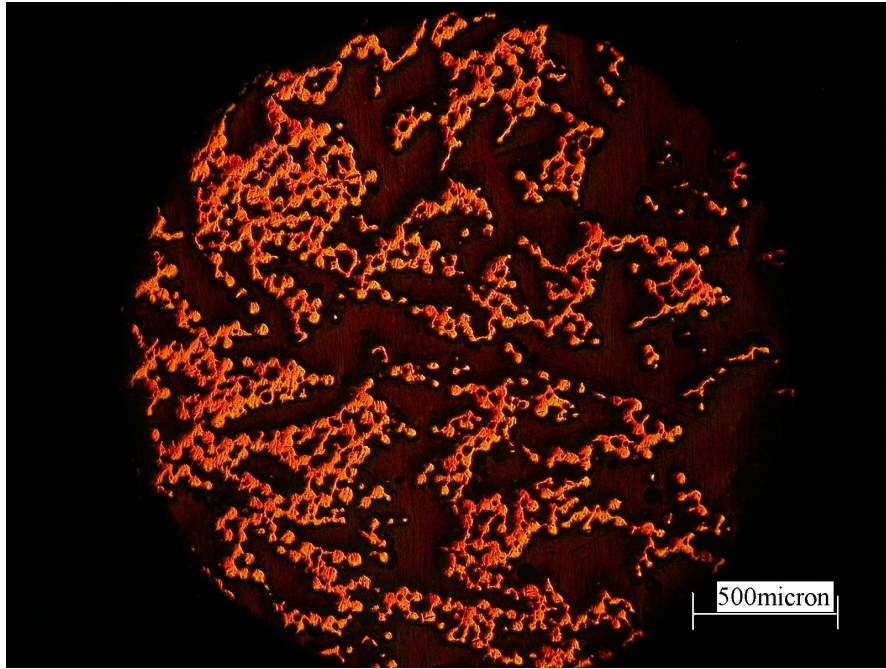
Figure 5.3.   Optical micrograph of the foam: P= 200 MPa, T=1200 ºC and t=2 h.
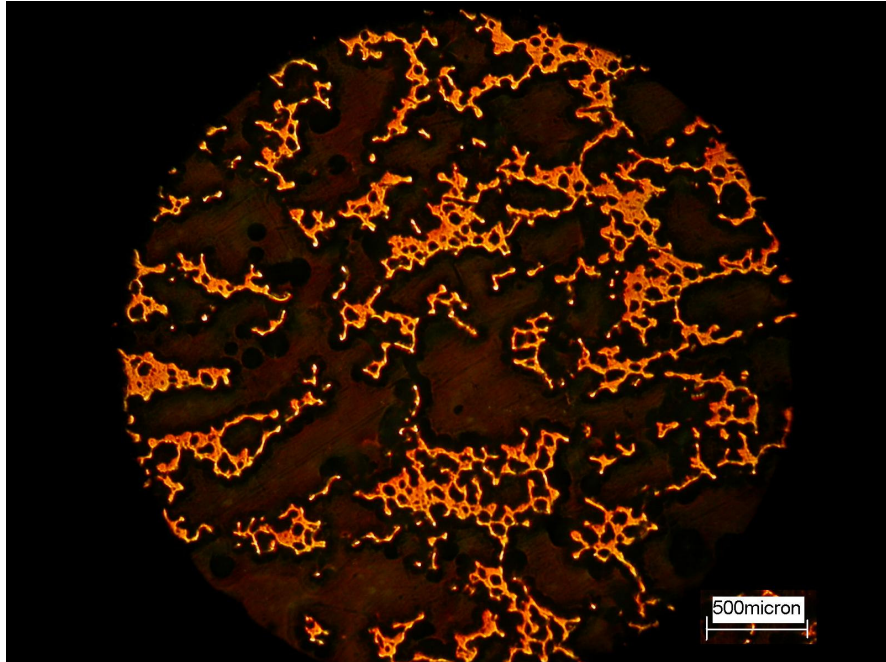
Figure 5.4.   Optical micrograph of the foam: P=300 MPa, T=1200 ºC and t=2 h.
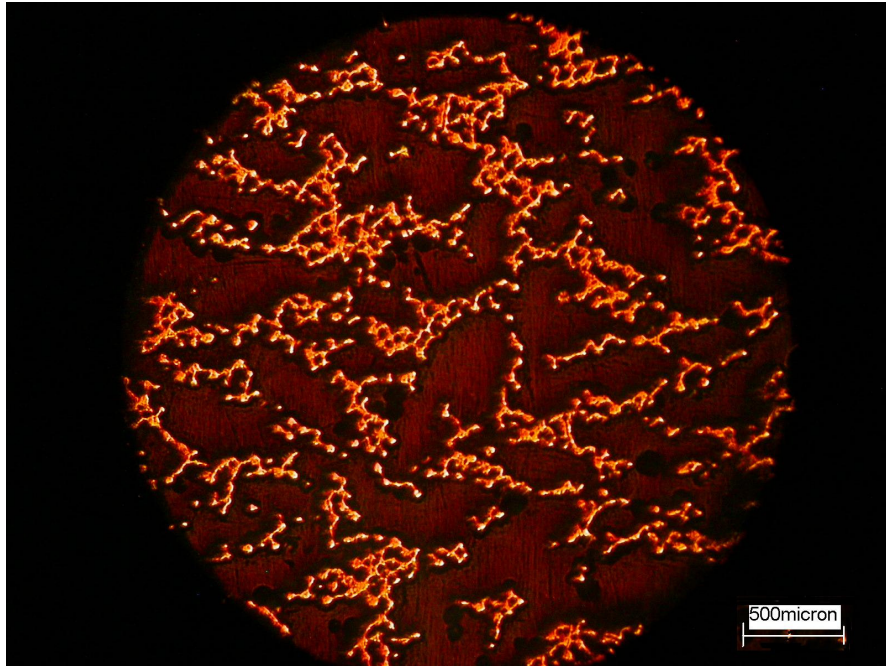
Figure 5.5.   Optical micrograph of the foam: P=400 MPa, T=1200 ºC and t=2 h.
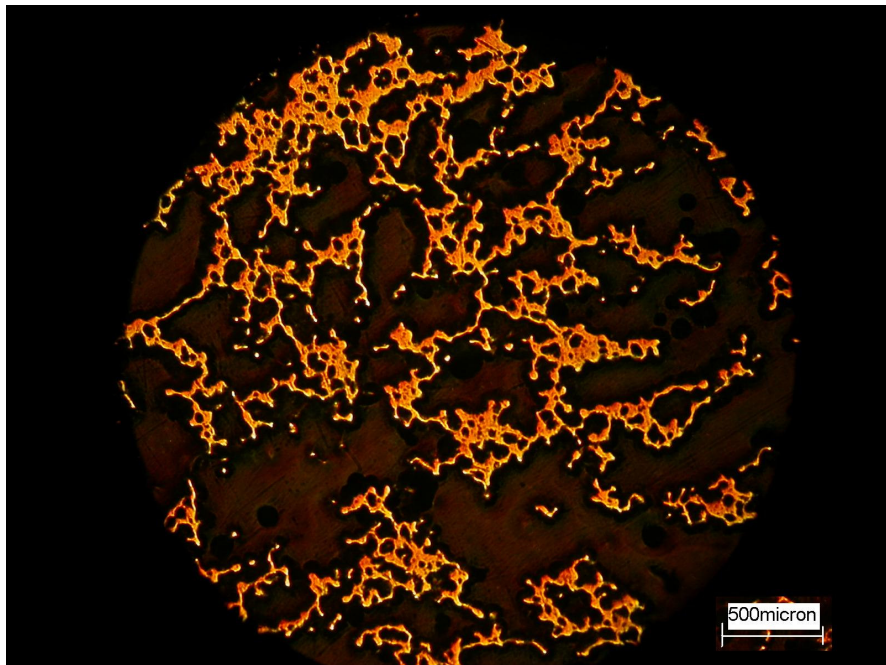
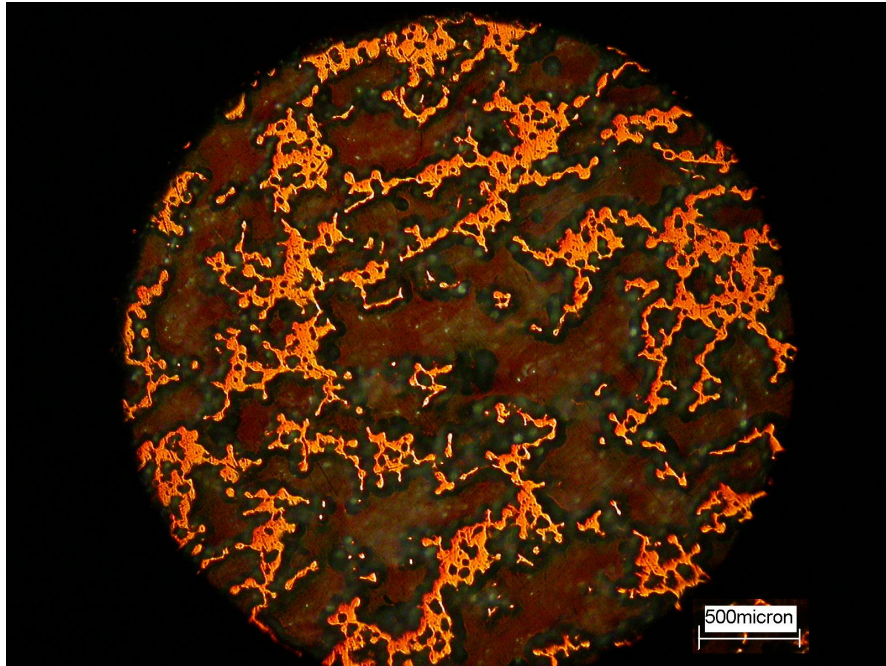Figure 5.6.   Optical micrograph of the foam: P=500 MPa, T=1200 ºC and t=2 h.

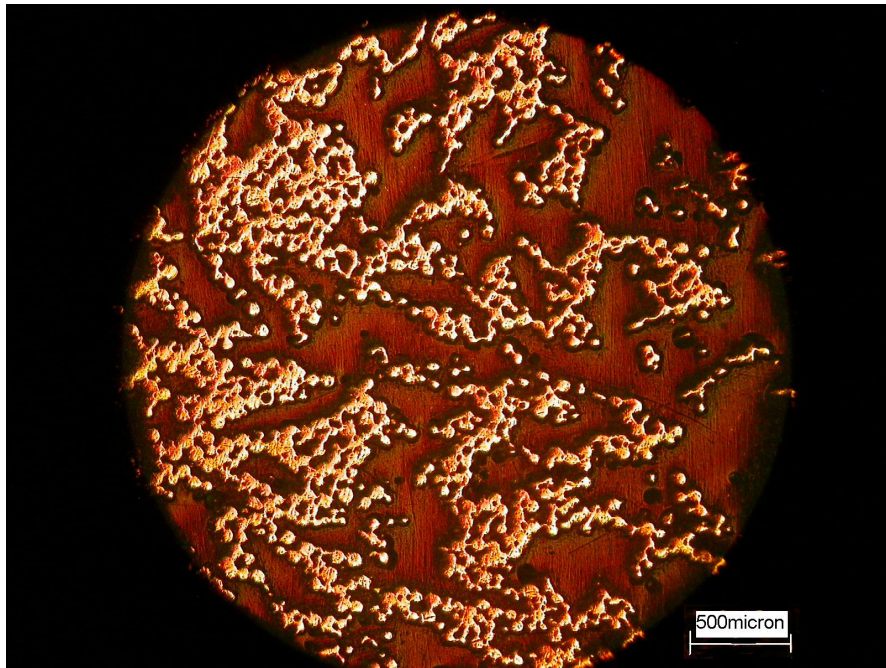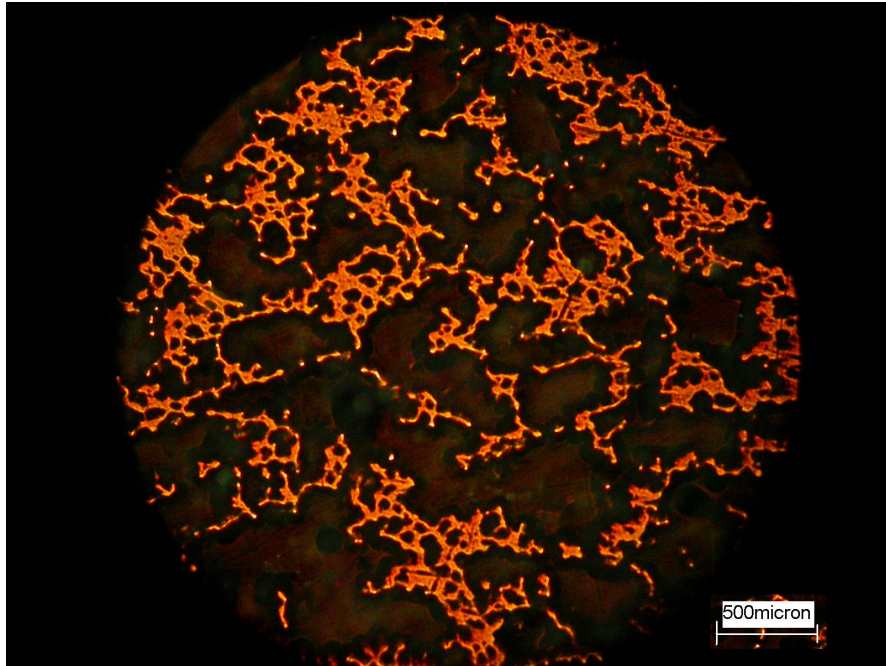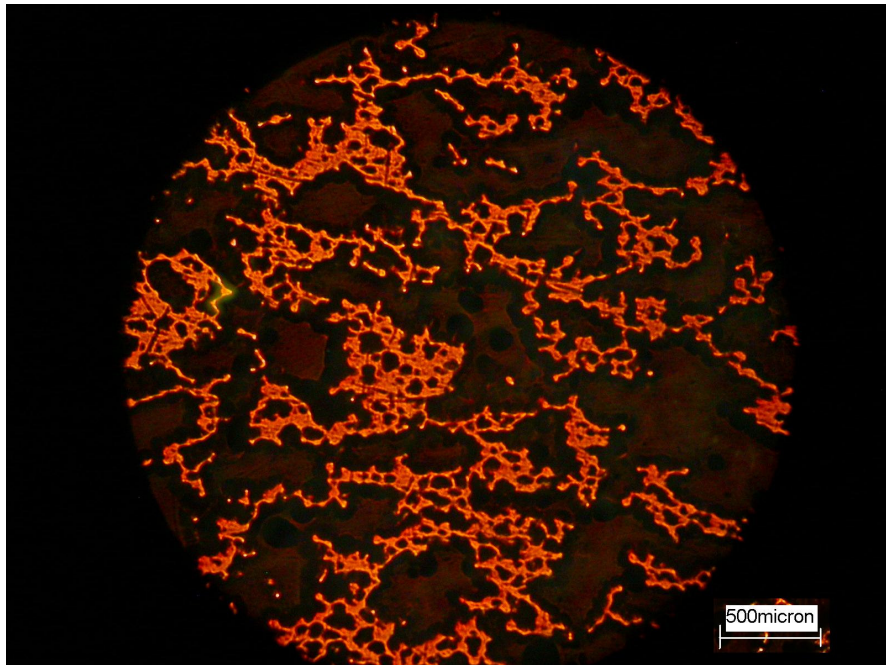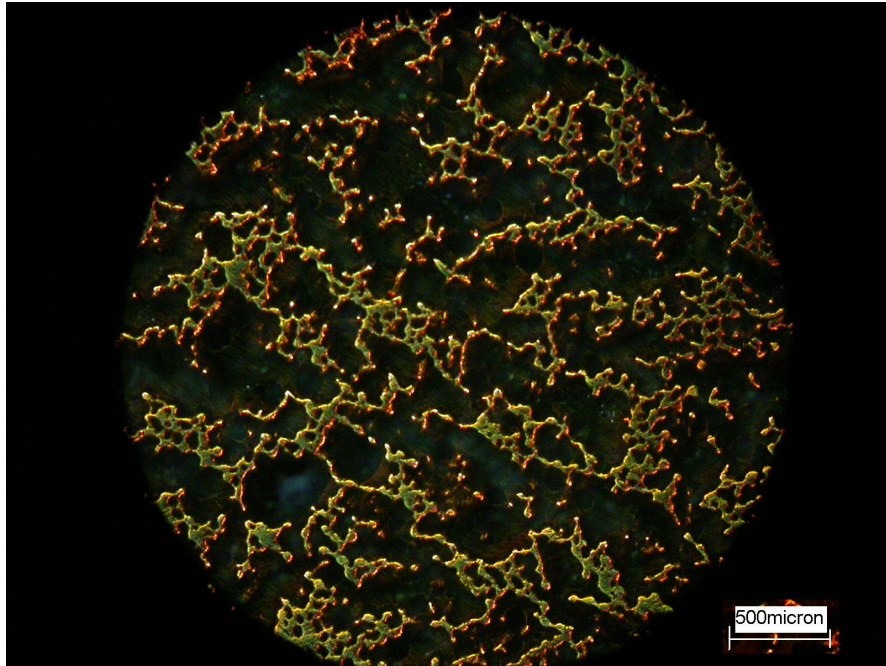Figure 5.7.   Optical micrograph of the foam: P= 300 MPa, T=1300 ºC and t= 2 h .

Figure 5.8.   Optical micrograph of the foam: P= 500 MPa, T=1300 ºC and t= 2 h.

Figure 5.9.   Optical micrograph of the foam: P=700 MPa, T=1300 ℃ and t=2 h.

Figure 5.10.   Optical micrograph of the foam: P= 700 MPa, T=1300 ℃ and t= 4 h.

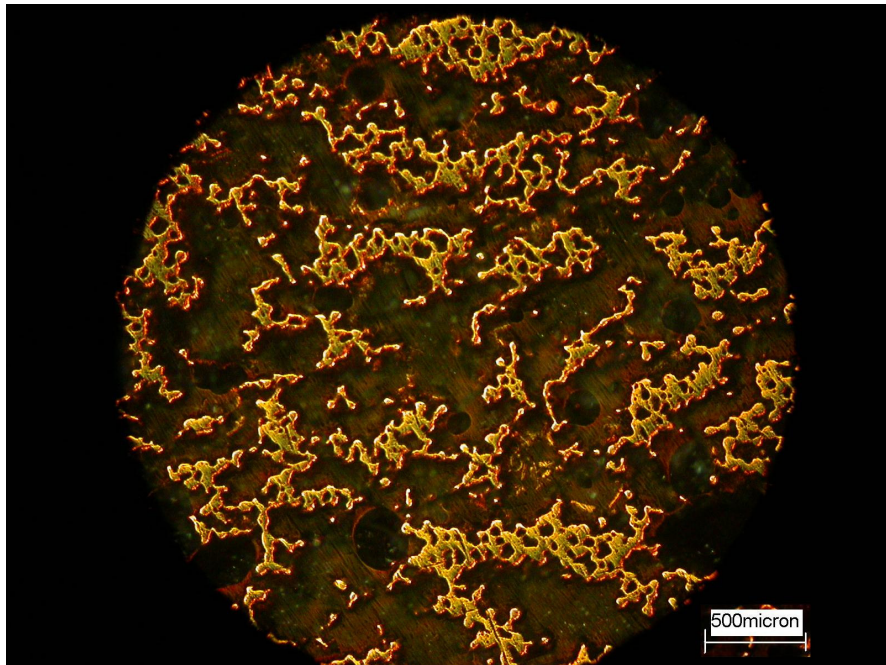Figure 5.11.   Optical micrograph of the foam: P=500 MPa, T=1300 ºC and t= 4 h.

Figure 5.12.   Optical micrograph of the foam: P=500 MPa, T=1300 ºC and t= 6 h.

5.4. Compression Mechanical Properties

The compressive stress-strain curves of the prepared foams at different compaction pressures are shown in Figures 5.13 to 5.16. The elastic modulus of the foams is determined in the initial region of stress-strain graph and the yield strength is taken as the proportional limit as shown in Figures 5.17 at the lowest compaction pressure (200 MPa) and shortest sintering time (2h), the foam shows a linear elastic region followed by catastrophic fragmentation of the sintered body which is reflected as the sudden decrease of the stress values after a maximum stress value ranging between 25 and 35 MPa as depicted in Figure 5.13. Figure 5.13 also shows the variations of the stress values between the four foam samples processed with the same parameters. The stress values vary 10 MPa between the samples at most but the strain at which fragmentation or sudden decrease in stress values starts are the same for the foam samples tested, around 0.07 strains. Figure 5.14, 15 and 16 show sequentially the compression stress strain curves of the foams compacted at 300, 400 and 500 MPa but sintered at the same temperature, 1200 ^{o}C, and sintering time 2 h. These figures clearly show that the foam show a trend of increasing maximum stress with increasing compaction pressure while the compaction pressure has negligible effects on the fragmentation of the foam at a relatively low strain. The increasing compressive stresses of the foams with increasing compaction pressure is seen in Figure 5.17 in which the representative stress-strain curves of the foams at 200, 300, 400 and 500 MPa compaction pressure are drawn altogether. The stress-strain curves of the foams sintered at 1200 ^{o}C for 2 h show relatively brittle foam behavior. The maximum compressive stress is around 40 MPa and even its value decreases as the compaction pressure decreases. It is also noted that these foams show also very low elastic moduli values, ranging between of 0.52 - 1,18 GPa, depending on the applied compaction pressure. The porosity values of these foams also ranges between 62 and 64% as listed in Table 5.1 The increase of the compressive stress of the foams with compaction pressure may be attributed to the reduced porosity levels with increasing compaction pressure. However, the brittle failure mode of foams dictates more or less that the bonding area between the sintered particles is not large enough or the bonding between particles is not strong enough to induce a ductile failure

mode of deformation composing of regions elastic deformation and cell collapse in the stress-strain curve.
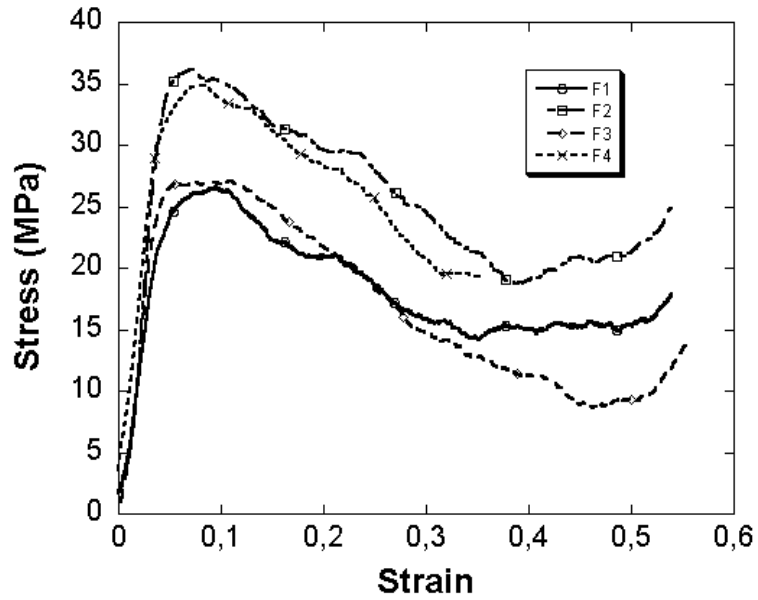

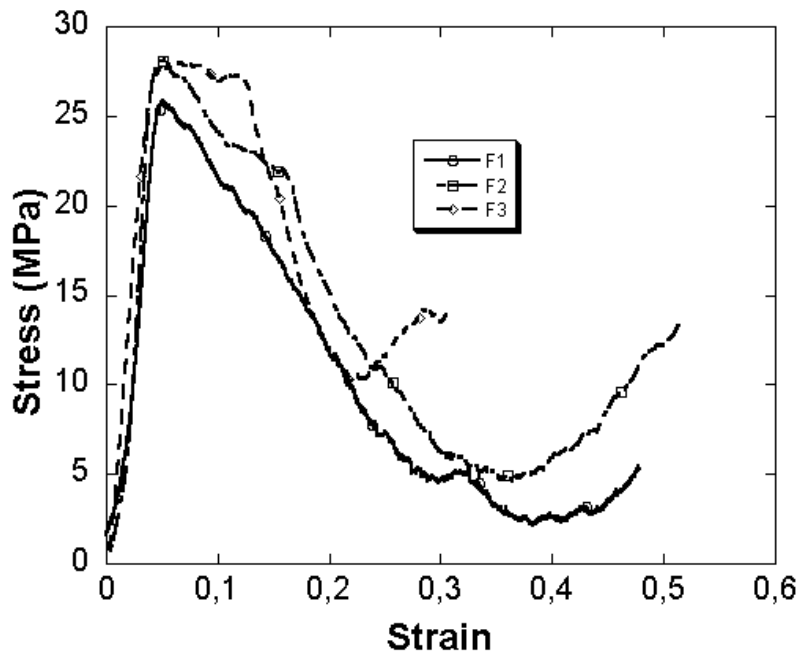Figure 5.13.   Compression stress-strain curves of the foam: P= 200 MPa, T=1200 ºC and t=2 h.

Figure 5.14.   Compression stress-strain curves of the foam: P= 300 MPa, T=1200 ºC and t=2 h.

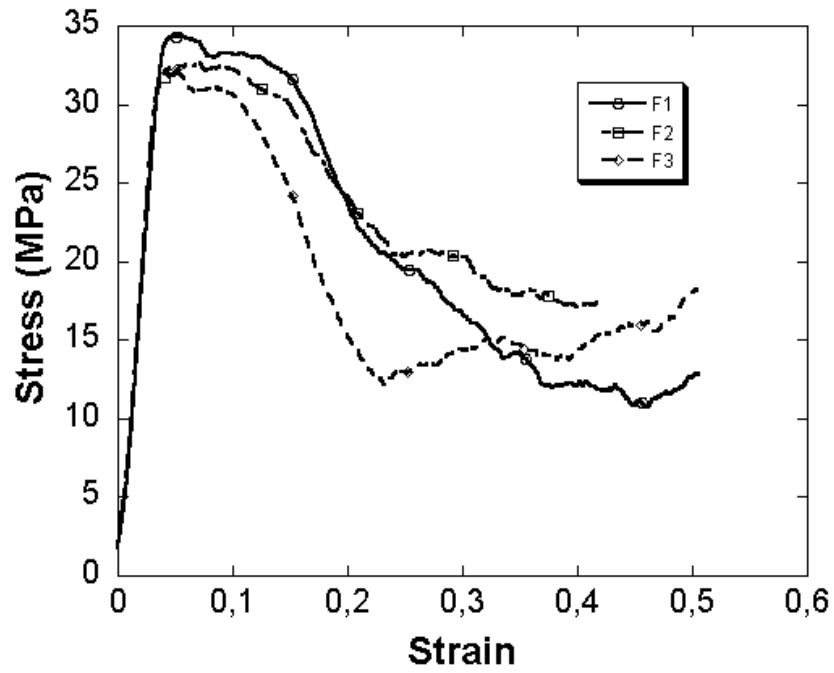Figure 5.15.   Compression stress-strain curves of the foam: P= 400 MPa, T=1200 ºC and t=2 h.
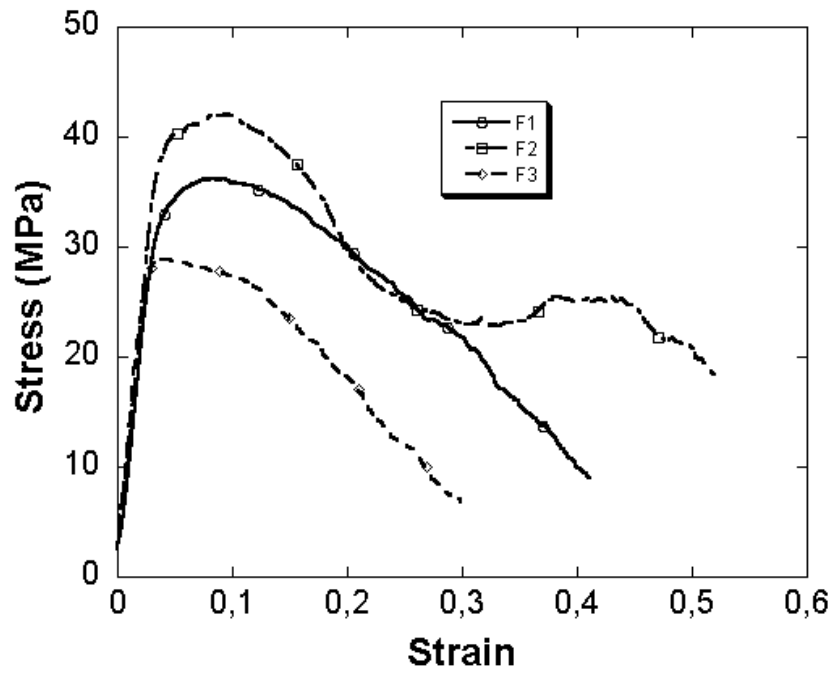
Figure 5.16.   Compression stress-strain curves of the foam: P= 500 MPa, T=1200 ºC and t=2 h.
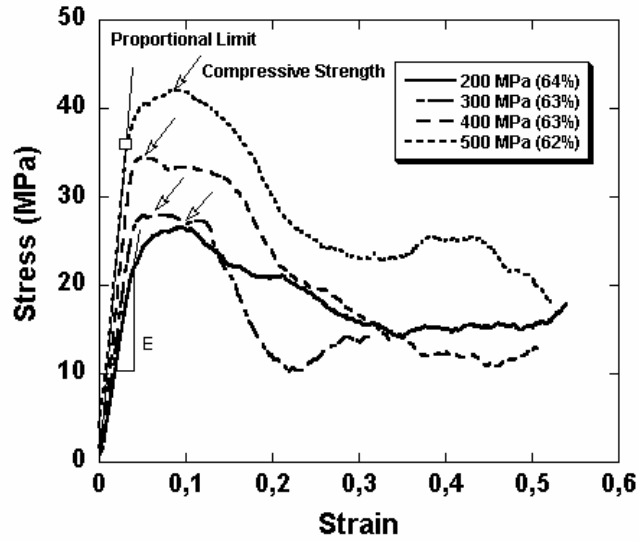
Figure 5.17.   Representative compression stress-strain curves of the foams: P=200, 300, 400, 500 MPa, P= 300 MPa, T=1200 ºC and t=2 h.
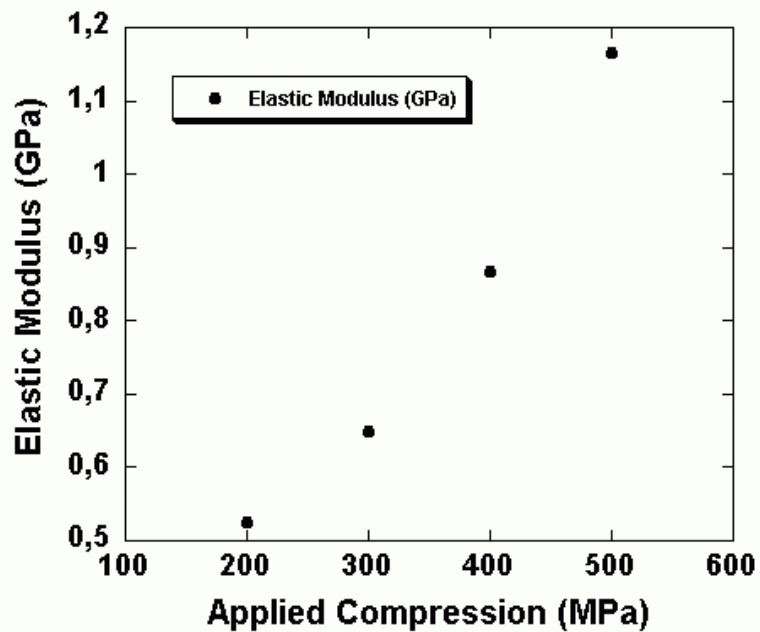

Figure 5.18. Variation of elastic moduli of the foams with the applied compaction pressure.

The compressive stress-strain curves of foams sintered at 1300 °C for 2 h are shown sequentially in Figure 5.19, 20 and 21 for the cold compaction pressures of 300, 500 and 700 MPa. Increasing sintering temperature comes with several effects in the compression behavior of the foam. First at low compaction pressures, 300 and 500 MPa although foam still show relatively brittle behavior the compressive stresses increases greatly as compared with that of the samples sintered at 1200 °C. The compressive stress ranges between 50 and 80 MPa for the compaction pressures of 300 and 500 MPa. Second, the sudden decrease in the stress values increases to larger strains, 0.2. Finally at 700 MPa, the foams show a typical ductile metal foam behavior composing of a linear elastic deformation region followed by an increasing foam collapse region. These foams samples did not fracture until about large strains, 0.6. The porosity level of the foam samples sintered at 1300 °C are 61, 60 and 58% for the compaction pressure of 300, 500 and 700 MPa as seen in Table 5.1. The sintering time decreased the foam porosity from 62% to 60% at a compaction pressure of 500 MPa.
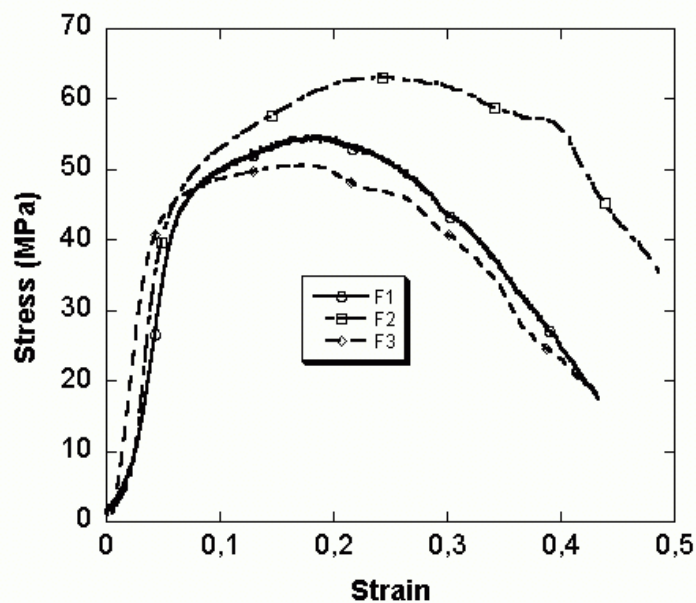

Figure 5.19.   Compression stress-strain curves of the foam: P= 300 MPa, T=1300 °C and
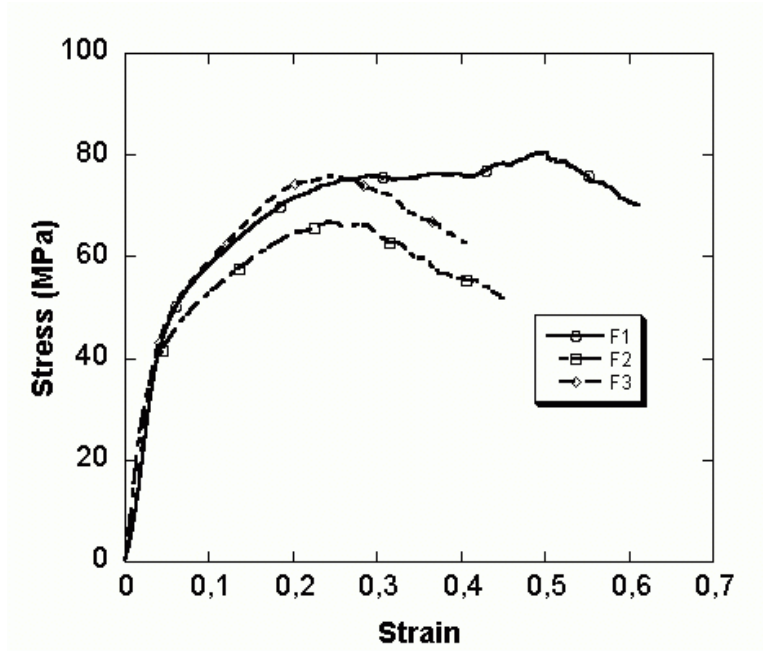t=2 h.

Figure 5.20.   Compression stress-strain curves of the foam: P= 500 MPa, T=1300 ºC and
                t=2 h.
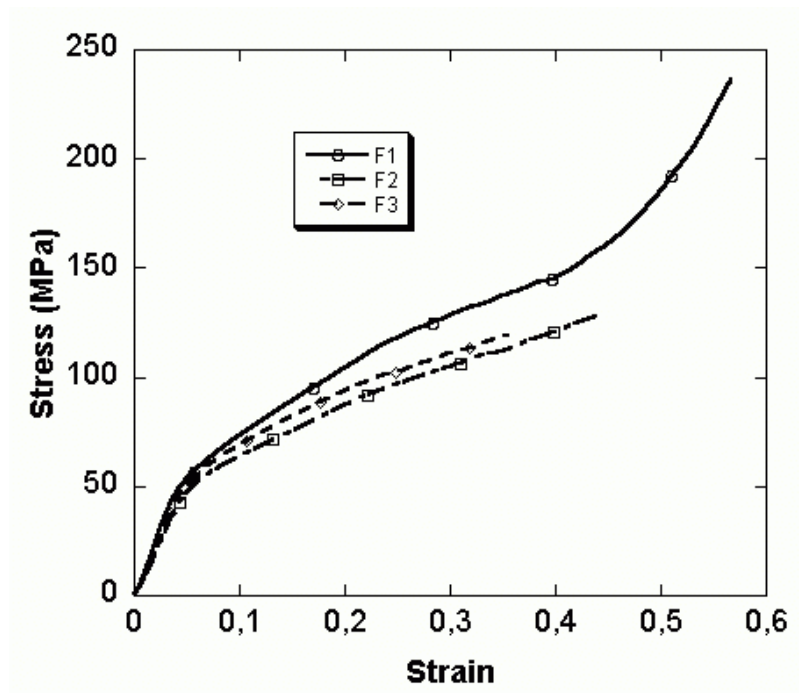
Figure 5.21.   Compression stress-strain curves of the foam: P= 700 MPa, T=1300 ºC and
                t=2 h.

Figure 5.22 shows the effect of sintering time on the stress-strain behavior of the foam sintered at 1300 º C and compacted at 700 MPa. Compared to 2 h sintering at 700 MPa pressure, the increasing sintering time induces a brittle foam behavior. While, increasing sintering time from 2 to 4 and 6 h at 1300 ºC in foam samples compacted 500 MPa reverts the brittle foam behavior into a ductile one as shown in Figure 5.23 and 5.24. at 6 h sintering time foam show increased yield stress as compared with that of the samples sintered at 4 h. The porosity levels of samples compacted 500 MPa and sintered for 4 h and 6 h are 61 and 58%, respectively. It should be noted that the initial volume percentages of the space holder is more or less reached after sintering.
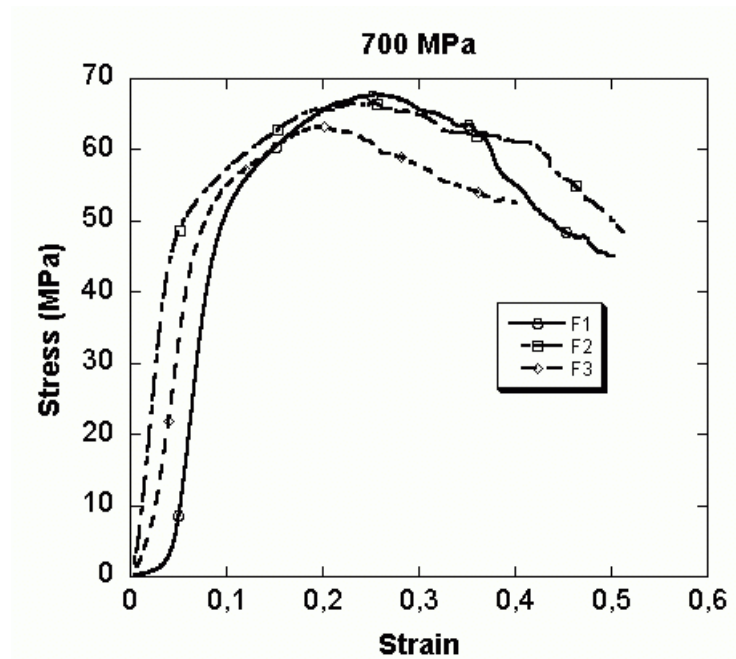

Figure 5.22.   Compression stress-strain curves of the foam: P= 700 MPa, T=1300 ºC and
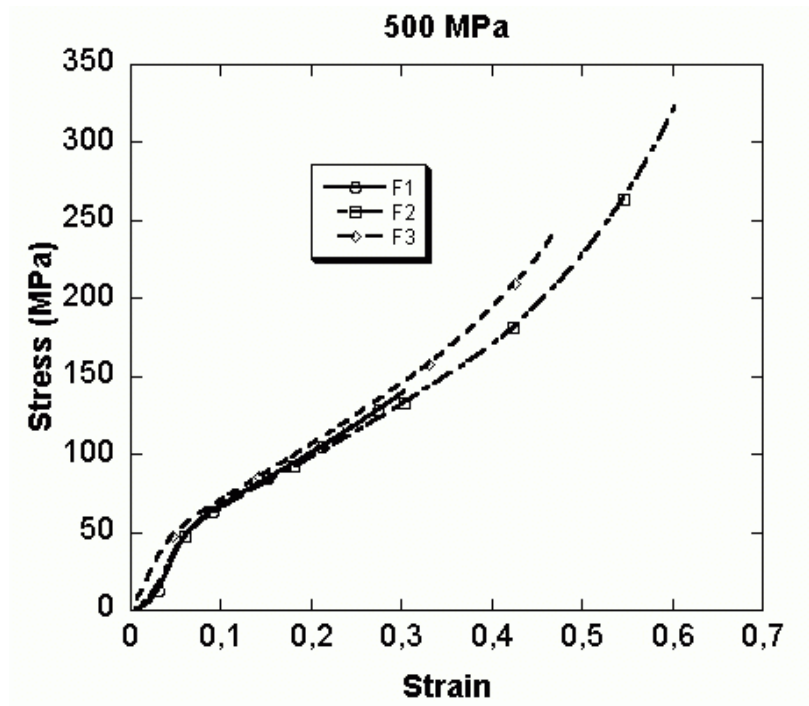   t=4 h.

Figure 5.23. Compression stress-strain curves of the foam: P= 500 MPa, T=1300 °C and t=4 h.
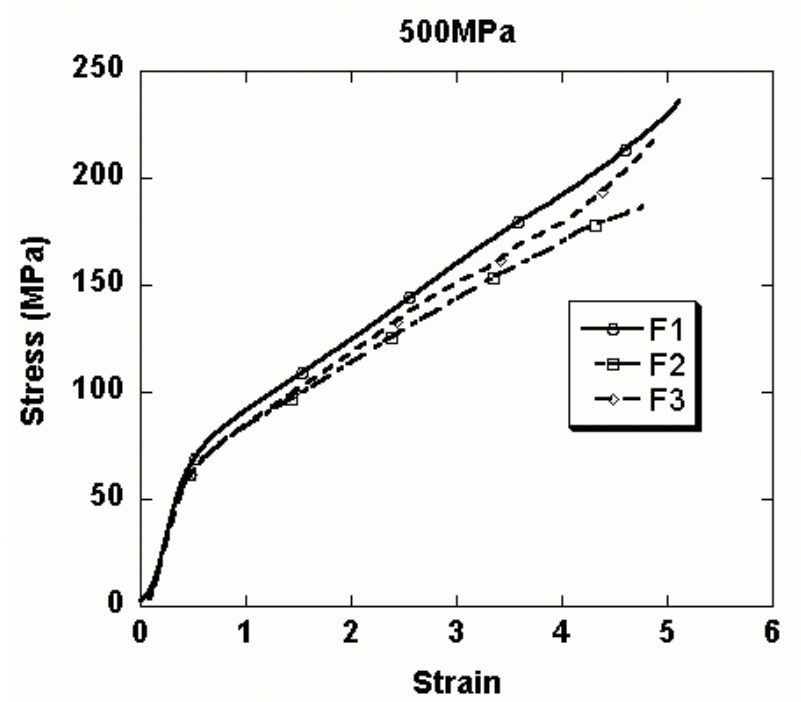
Figure 5.24.   Compression stress-strain curves of the foam: P= 500 MPa, T=1300 °C and
t=4 h.

Several trials were also performed by changing the initial space folder volume percentages, 52% and 72% while keeping the compaction pressure 500 MPa and sintering time 6 h. These foams show also brittle behavior, showing that compaction pressure and sintering time and temperature should be optimized for any specific volume percentages of the space holder.

5.5. Effect of Porosity on the Yield Strength

The variation of the yield strength of the foam with porosity is shown in Figure 5.25. It should be noted here the data shown in this figure belong to the samples compacted at 500 MPa and sintered at 1300 °C. Therefore the variation of the porosity levels simply arises due to the change of the sintering time. It is shown in the same figure both porosity level and yield strength are affected by the sintering time. Three percent decrease in porosity results in 20 MPa increase in the yield strength as depicted in Figure 5.25

38

relatively high value of stress increase with porosity may be attributed to effects. The lower porosity levels naturally tend to increase the stress values since more solid is accommodated in the foam structure. However the enhanced bonding between particles at increasing sintering times may have also contribution to the foam strength.
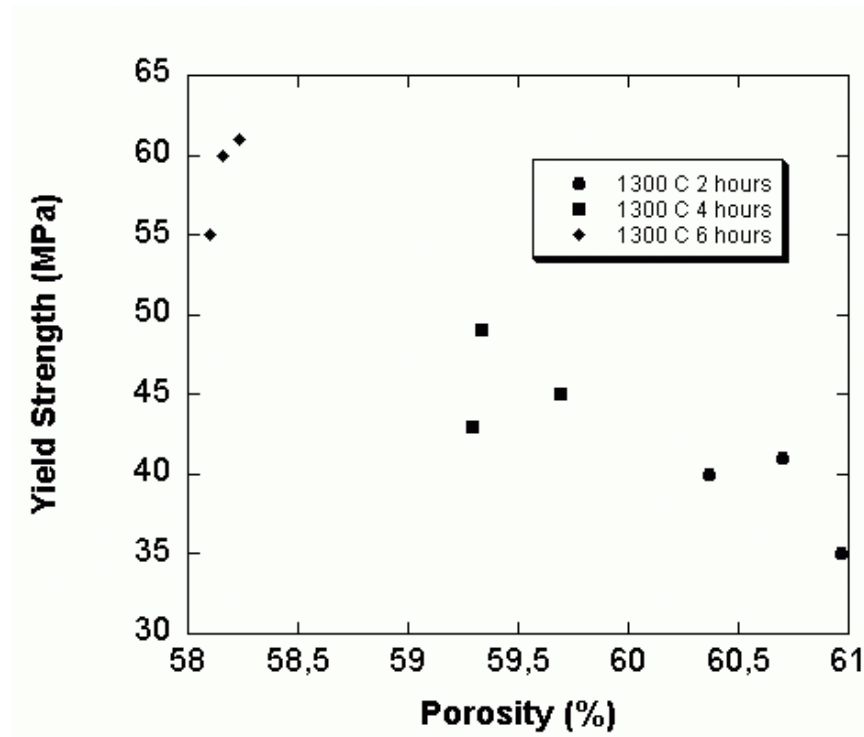

Figure 5.25.   Variation of the yield strength with the porosity.

5.6. Microscopic Studies

Microscopic studies have shown that the sintered powders have Widmanstätten structure. In this structure, colonies of β lathes (bcc and rich in V) and α platelets (hcp and rich in Al) formed inside the prior β grains (Figure 5.26 (a) and (b)). The percentage and thickness of β phase were measured typically 18-20% and 0.2-1 μm, respectively. The

thickness of α platelets varied between 4 and 8 μm and it was also microscopically observed that the thickness of α platelets increases at and near the interparticle bond region.


(a)

Element	Wt%
Al	4.65
V	10.75
Ti	89.72

| Element	Wt%
Al	7.34
V	2.93
Ti	89.72
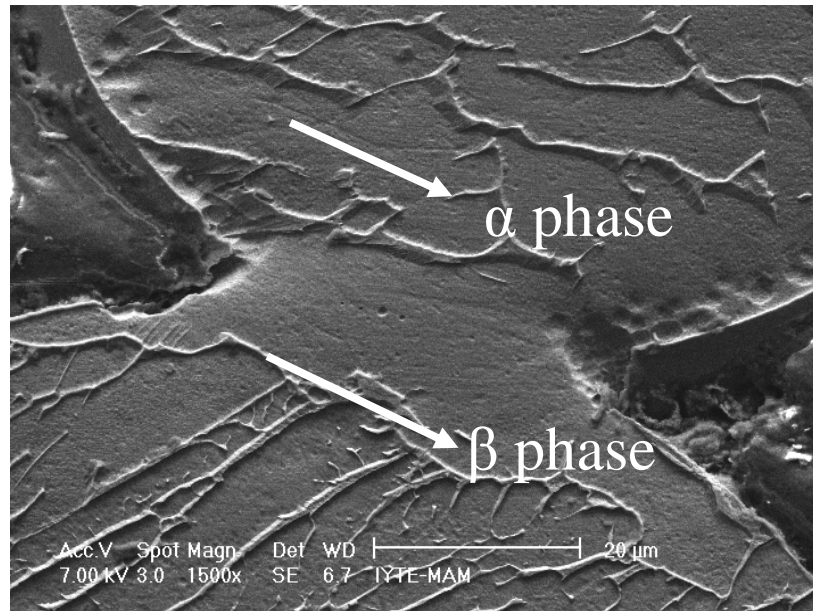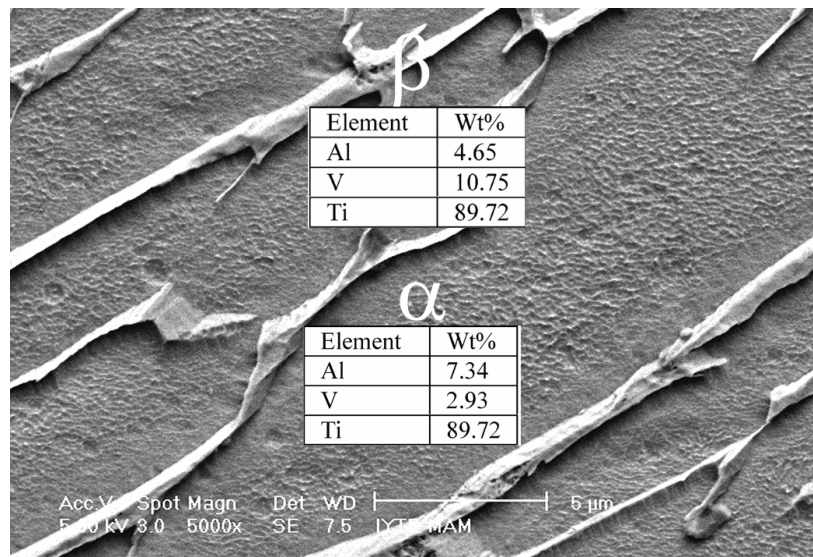
(b)

Figure 5.26.   SEM image showing Widmanstätten microstructure of sintered foam sample and (b) magnified image of Widmanstätten microstructure showing α and β.
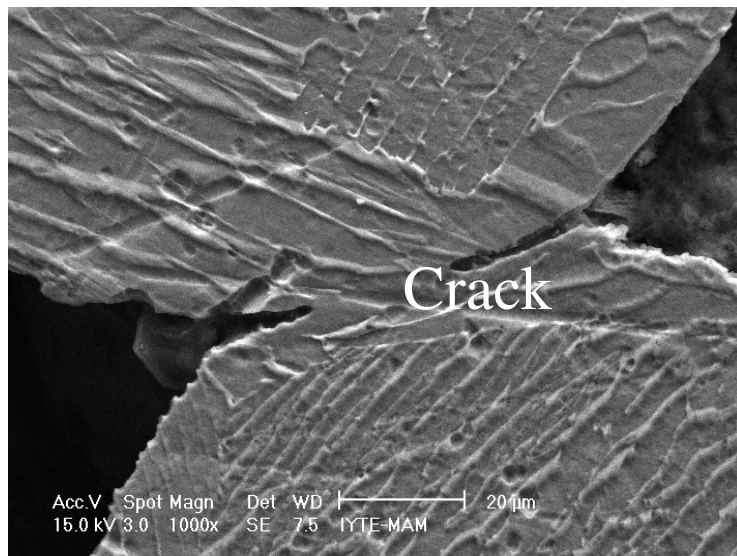
Figure 5.27 (a) and (b) show the interparticle regions in the untested samples sintered at 1200 and 1300 $^\circ$C, respectively. The particle structures show similar microscopic features. It is observed that the failure starts from the interparticle regions, as depicted in Figure 5.27 (c) for a deformed foam sample. Figures 5.28 (a) and (b) show the optical microscope micrographs of unetched and etched sample compacted at 500 MPa and sintered at 1300 $^\circ$C for 6 h. Two different sizes of the pores are clearly seen in these figures. The larger pores, 400 micron, are due to the space holder removal and smaller pores ranging between 10-20 micron form between the particles. The sizes of the interparticle pores however were observed to increase at lower compaction pressures. It was also observed that high compaction pressure resulted in particle deformation as depicted in Figure 5.28 (a).
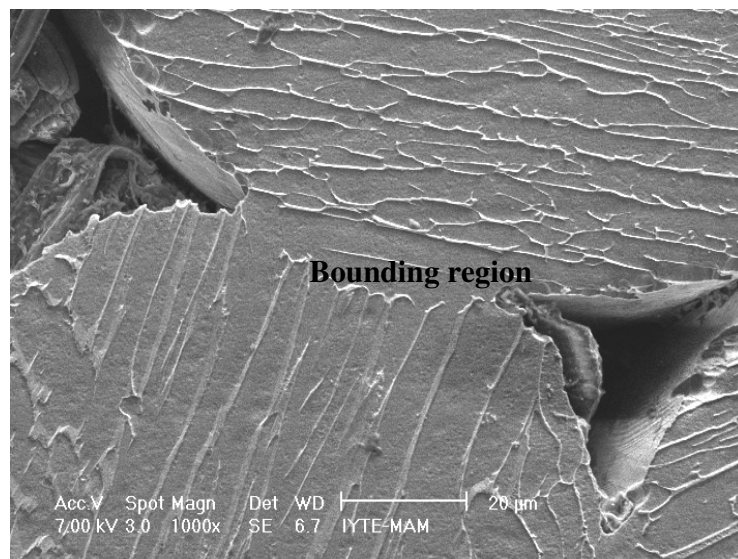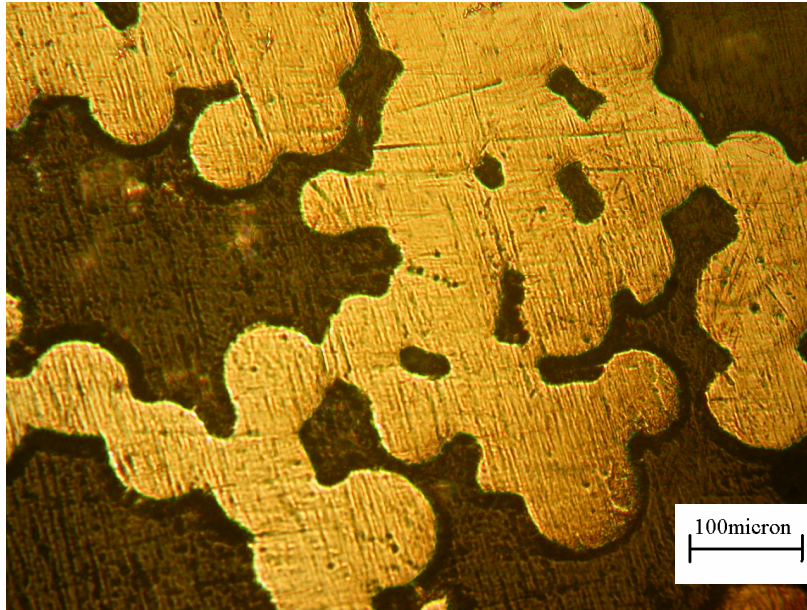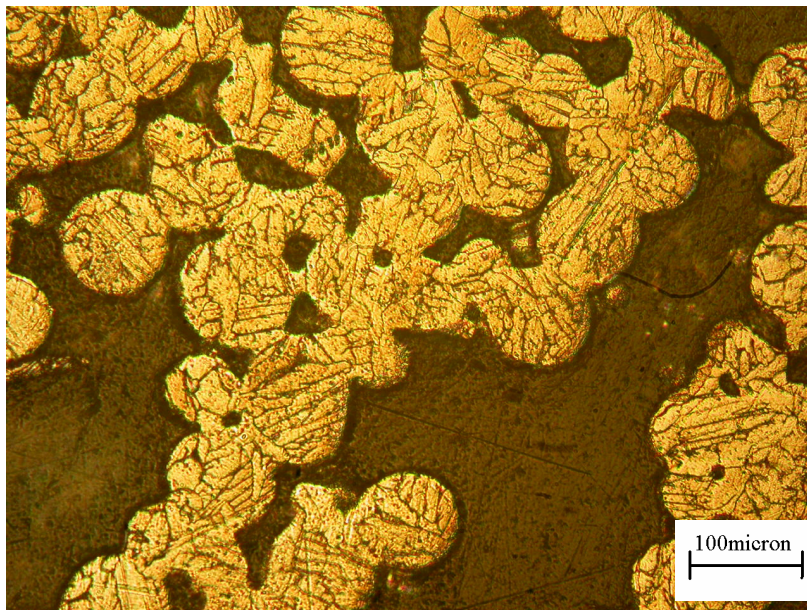

(a)
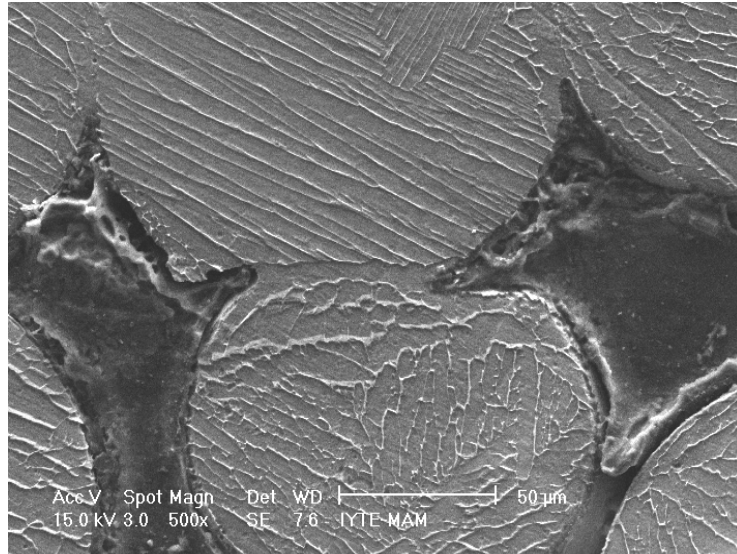
(b)

(c)

Figure 5.27.   Interparticle regions of the foams (a) P=200 MPa, T=1200 ºC and 2 h and (b) and (c) P=300 MPa, T=1200 ºC and 2 h.

(a)

(b)

Figure 5.28.   Optic microscopy images of the foam (a) before etching and (b) after etching, P=500 MPa, T=1300 ºC and t= 6 h.
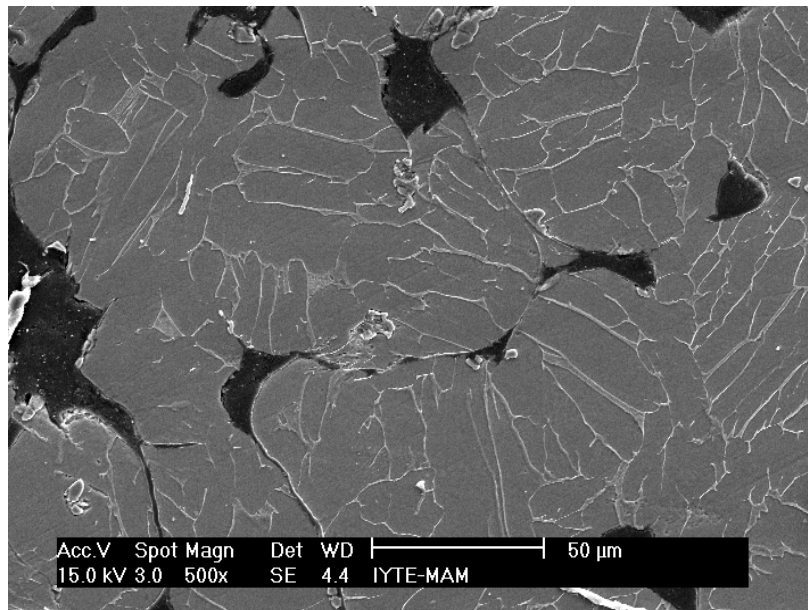
Figure 5.28.   SEM image of the foam: P=500 MPa, T=1300 °C and t= 6 h.

In Figure 5.29, undeformed and deformed images of the foam compacted at 500 MPa and sintered at 1300 °C for 6 h are shown. The foam show localized deformation starting from the mid-sections. This deformation matches with the ductile metal foam deformation.

For about 60% porosity ductile foam behavior are found in the samples compacted at 500 MPa and sintered at 1300 °C for 6 h. Since higher compaction pressure may induce deformation of space holder, 700 MPa compaction pressure are disregarded. Using above parameters prototype cervical cages were produced as seen in Figure 5.30. These cages are further mechanically tested in order to satisfy the mechanical requirements of the human cervical system. Animal tests will be also performed.

Figure 5.29.   Undeformed and deformed images of the foam: P= 500 MPa, T=1300 ℃, t=6 h.
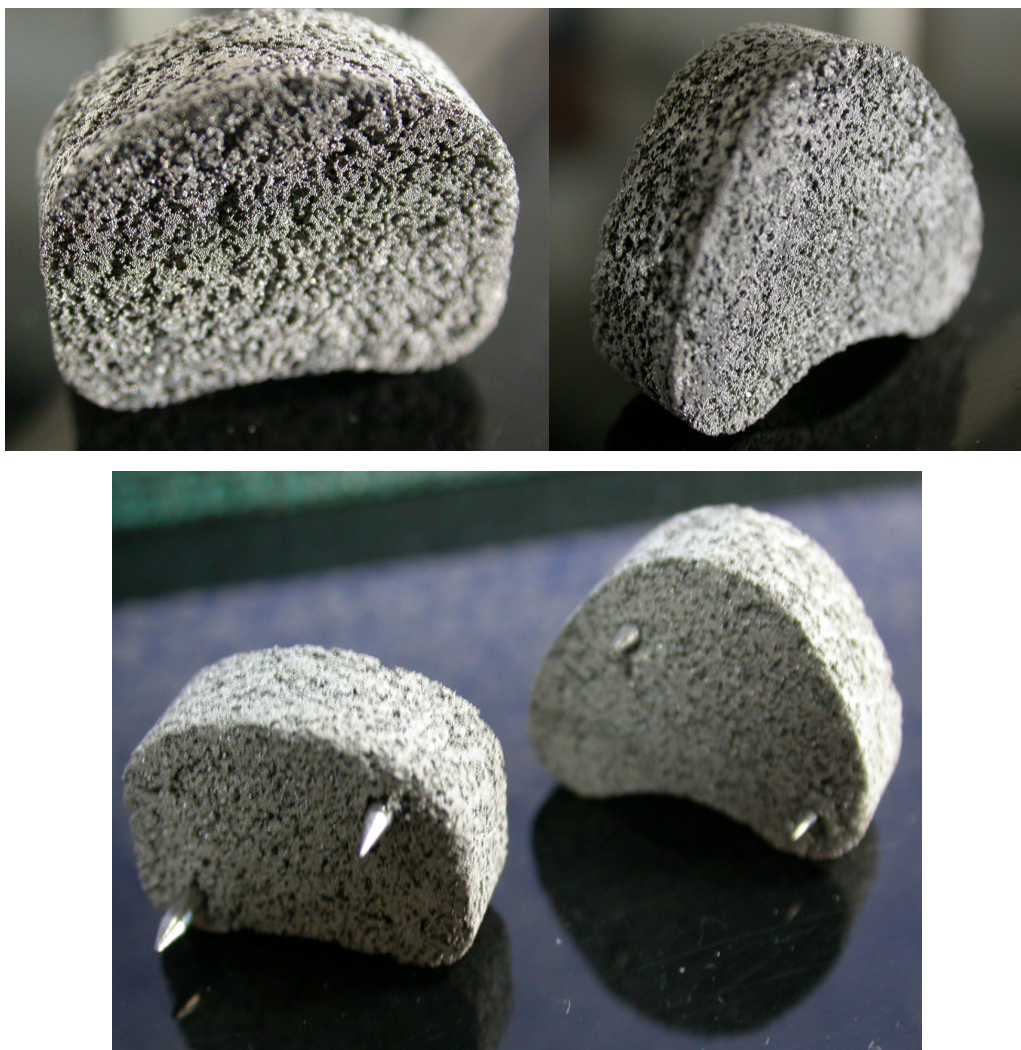
Figure 5.30   Cervical Cages (cold compaction pressure at 500 MPa, T=1300 ºC, 6 h.

CONCLUSIONS AND RECOMMENDATIONS

Sintered powder foams of Ti6Al4V alloy were prepared in the porosity around 60% using atomized spherical powders by varying the cold compaction pressure, sintering temperature and time. Cylindrical green powder compacts were cold compacted at various pressures and then sintered at 1200 ^{o}C and 1300 ^{o}C for 2, 4 and 6 hours. The final porosities and average pore sizes were determined as functions of the applied compaction pressure. The mechanical properties were investigated through compression testing at quasi-static strain rate. Microstructural analysis of as-received powder and sintered untested and tested foam samples were performed in order to investigate microstructure development after sintering and deformation and failure mechanisms under compressive loads.

The compression behavior foamed Ti alloy metal varied with cold compaction pressure, sintering temperature and sintering time. Foams compacted at 200, 300, 500 sintered at 1200 ℃ for 2 h showed brittle failure, while compacted at 700 MPa and sintered at 1200 ℃ for 2 h showed ductile failure. Similarly, foams compacted at 500 MPa and sintered at 1300 ℃ for 4 and 6 h showed typical foam metal compression behavior composing localized deformation region and increasing plato stress. Microscopic analysis have show that two ranges of pore size. Larger pore size around 400 micron resulted from the space holder removal while small size pore range, 0-20 micron formed between interparticle regions. The brittle foam behavior at lower compaction pressures and sintering temperature and times was attributed to the weak interparticle bonding. The results of this study were used to prepare cervical cages with a porosity of about 60% and pore size of 400 micron.

REFERENCES

Banhart, J., 2001, Manufacture, characterization and application of cellular metals and metal foams. *Prog. Mater. Sci.* 46:559-632.

Chang, Y., Oka, M., Kobayashi, M., Gu, H., Li, Z., Nakamura, T., and Ikada, Y., 1996, Significance of interstitial bone ingrowth under load-bearing conditions: a comparison between solid and porous implant materials, *Biomaterials* 17: 1141-1148.

Clemow, A. J. T, Weinstein, A. M., Klawitter, J. J., Koeneman, J., and Anderson, J., 1981, Interface mechanics of porous titanium implants. *J. Biomed. Mater. Res.* 15: 73-82.

Elbir, S., Yılmaz, S., Toksoy, K., Guden, M., and Hall, I. W., 2003, SiC-particulate aluminum composite foams produced by powder compacts: Foaming and compression behavior, *J. Mater. Sci.* 38:4745-4755.

Gibson L. J., and Ashby F., 1997, *Cellular solids: structure and properties.* Cambridge University Press.

Körner, C., and Singer, R. F., 2002, Processing of metal foams-challenges and opportunities. *Adv. Eng. Mater.* 2:159-165.

Kulkarni SB, Ramakrishnan P. Int J Powder Met 1973; 9:41

Martin, B., Stiller, C., Buchkremer, H. P., Stöver, D., and Baur, H., 2000, High purity titanium, stainless steel and superalloy parts . *Adv. Eng. Mater.* **2**:196-199.

Pillar, R. M., 1987, Porous-surfaced metallic implants for orthopedic applications. *J. Biomed. Mater. Res.* 21:1-3.

WEB_1, 2002. Froes, F. H., Lightweight heavyweight, *Metal Powder Report* (http://*www.metal-powder.net).*

Wen, C. E., Mabuchi, M., Yamada, Y., Shimojima, K., Chino, Y., and Asahina, T., 2000 , Processing of biocompatible porous Ti and Mg. *Script. Mat.* 45:1147-1153.

Wen, C. E., Yamada, Y., Shimojima, K., Chino, Y., Asahina, T., and Mabuchi, M., 2001, Processing and mechanical properties of autogenous titanium implant materials. *J. Mater. Sci.* 13:397-401.

Weiner, S., and Wagner, H. D., 1998, The material bone:structure-mechanical function relations. *Annu. Rev. Mater. Sci.* 28:271-298.